Simple colorimetric copper(II) sensor – spectral characterization and possible applications

Błażej Galiński[1], Jarosław Chojnacki[2], Ewa Wagner-Wysiecka[1,3]*

[1]Department of Chemistry and Technology of Functional Materials, Faculty of Chemistry, Gdańsk University of Technology, Narutowicza Street 11/12, 80-233 Gdańsk, Poland

[2]Department of Inorganic Chemistry, Faculty of Chemistry, Gdańsk University of Technology, Narutowicza Street 11/12, 80-233 Gdańsk, Poland

[3]Advanced Materials Center, Faculty of Chemistry, Gdańsk University of Technology, Narutowicza Street 11/12, 80-233 Gdańsk, Poland

Highlights

- New *o*-hydroxyazocompound **L** has been obtained
- **L** was investigated as spectrophotometric colorimetric chemosensor for copper(II)
- **L**-based test strips and cotton swabs can colorimetrically detect copper(II) in water
- **L**-based copper(II) selective optodes were proposed

Graphical abstract
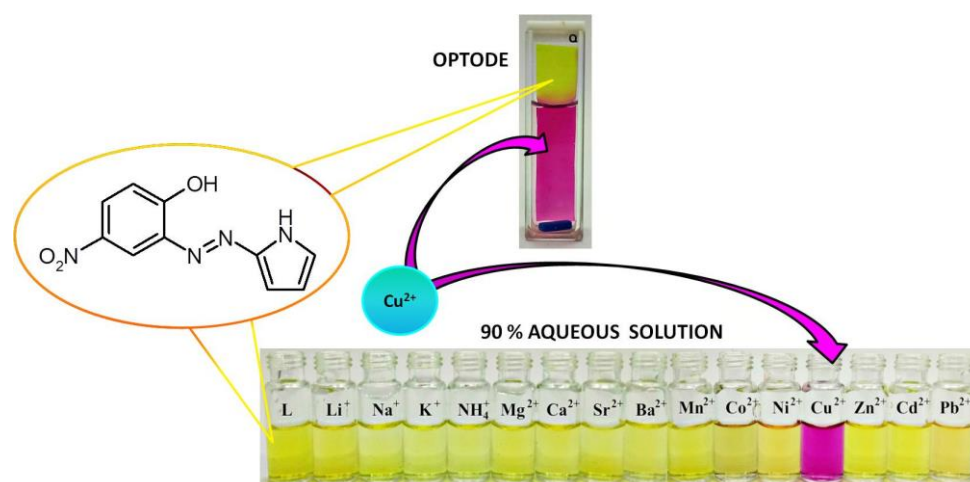
Abstract

New *o*-hydroxyazocompound **L** bearing pyrrole residue was obtained in the simple synthetic protocol. The structure of **L** was confirmed and analyzed by X-ray. It was found that new chemosensor can be successfully used as copper(II) selective spectrophotometric regent in solution and can be also applied for the preparation of sensing materials generating selective color signal upon interaction with copper(II). Selective colorimetric response towards copper(II) is manifested by a distinct color change from yellow to pink. Proposed systems were effectively used for copper(II) determination at concentration level 10^{-8} M in model and real samples of water.

Keywords

copper(II), optical sensing, chromoionophore, azocompound, pyrrole

1. Introduction

Copper(II) is an essential and third most abundant transition metal ion in human body and plays a unique physiological role in animals and plants [1-4]. However, an excess as well as a deficiency of copper with respect to a critical level may cause many disorders in human body like for example Alzheimer's, Menkes and Wilson diseases [5-10] and also can be poisoning for animals and plants [11-13]. Because of toxic nature of copper(II) above a certain level of concentration, WHO has set maximum permissible limit of copper(II) in drinking water as 2.0 mg/L (3.15×10^{-5} M) [14]. Therefore, the detection of copper(II) in the various type of samples, e.g. environmental, biological, like body fluids, is important and essential. Various spectroscopic and electrochemical methods can be used for the detection and determination of metal ions in aqueous samples [15-20]. An elegant and comprehensive review on chemical, polymer and nanoparticle copper(II) colorimetric and/or fluorimetric sensors has been recently published [21]. The choice of the method depends on many factors such as for example the type of the sample, the concentration level of analyte. Often also the economic criterion is taken into consideration. Thus, besides the selectivity and sensitivity of sensor, also the price of the instrumentation and overall costs of the analysis are important. In this respect chemical sensors, including optical ones, can compete with most of the instrumental analytical methods. The operation of sensors can be based on different mechanisms of the generation of the analytical signal. One of them is chemical recognition of the analyte taking place in the receptor layer of the sensor. The process of chemical recognition relies on the affinity of the particular receptor towards analyte according to the rules of host-guest chemistry – one of the research area of supramolecular chemistry, where the design and synthesis of ion receptors for analytical purposes is one of the goals [22-32]. Important analytes include heavy metal cations [33-39], which have a significant impact on human health and the environment. Properly designed receptors of chromoionophoric properties can be components of sensing optical materials for the detection and determination of these ions in an aqueous medium [40-44]. Azo compounds due to their relatively simple synthesis, spectral and complexing properties constitute a promising group of such chromoionophores [45-47]. Essential receptors of heavy metal cations are often compounds bearing heterocyclic moieties [21]. Due to the various reactivity and photophysical properties, heterocyclic receptors containing nitrogen atoms are described as one of the best systems for the detection and determination of heavy metal ions [48, 49]. The interaction of heavy metal ions with the receptor can generate an optical signal that is measurable using spectrophotometric methods [50], but also solutions where the use of mobile

3

detection systems e.g. Smartphone-based detection devices [51-54] that use digital color analysis [55-62].

Here we present a facile synthesis and spectral characterization of simple *o*-hydroxyazocompound **L** bearing pyrrole residue. Newly obtained compound was characterized with the use of spectroscopic methods and investigated as a copper(II) receptor in organic solvents, mixtures of these solvents with water and in systems of complex ionic matrix, namely artificial body fluid and artificial urine. It has also been tested as a component of optical sensing materials for selectivity, sensitivity, regenerability, pH effect, limit of detection, interfering ions effect and lifetime. Tests were carried out to assess the possibility of using the prepared materials for the detection and determination of copper(II) in model and real samples of water.

2. Experimental

2.1. Reagents and materials

All chemicals of the highest available purity were purchased from commercial sources and used without further purification. Lithium perchlorate, sodium perchlorate monohydrate, bis(2-ethylhexyl) phthalate (DOP) and dibutyl phthalate (DBP) were obtained from Fluka. Potassium perchlorate, barium perchlorate, cobalt(II) perchlorate hexahydrate, nickel(II) perchlorate hexahydrate, copper(II) perchlorate hexahydrate, zinc perchlorate hexahydrate, lead(II) perchlorate trihydrate, tetrabutylammonium hydroxide 30-hydrate (TBAOH), *p*-toluenesulfonic acid monohydrate (TsOH), uric acid, creatinine, bis(1-butylpentyl) adipate (BBPA), 2-nitrophenyl octyl ether (NPOE), bis(2-ethylhexyl) sebacate (DOS), cellulose triacetate (CTA), triethylene glycol (TEG), potassium tetrakis(4-chlorophenyl)borate (KTClPB), acetonitrile (ACN), dichloromethane (DCM) and methanol (MeOH) were acquired from Sigma Aldrich. Magnesium perchlorate, calcium perchlorate hydrate, strontium perchlorate trihydrate and cadmium perchlorate hexahydrate were purchased from Alfa Aesar. All inorganic salts, hydrochloric acid, nitric acid, sodium hydroxide, disodium ethylenediaminetetraacetate dihydrate (EDTA), sodium citrate dehydrate, dipotassium oxalate monohydrate, urea, tris(hydroxymethyl)aminomethane, dimethyl sulfoxide (DMSO), acetone, 2-propanol, and filter papers were obtained from POCh. Glass microfiber filter Whatman GF/C was acquired from Schleicher & Schuell. TLC glass plates 60 RP-18 F_{254} and silica gel 60 (0.063 - 0.200 mm) for column chromatography were purchased from Merck. For measurements performed in mixed, water containing systems, deionized water (conductivity <1 $\mu S \cdot cm^{-1}$, Hydrolab) was used. For recovery studies Standard Reference Solution of copper(II) 1000 ppm (Merck) and Qnova calibration solution were used. Copper(II)

4

concentration for comparative studies was determined using the ICP-OES method with iCAP 7400 Analyzer. Mineral water samples were commercial bottled ones purchased from regular stores. Tap water samples were taken from local domestic sources of Pomerania (sample 1) and Warmian-Masurian (sample 2 and 3) Voivodeships (Poland).

2.2. Apparatus

^1H and ^{13}C spectra were recorded on Varian INOVA 500 spectrometer at 500 MHz and 125 MHz, respectively. Chemical shifts are reported as δ [ppm] values in relation to TMS. HR MS mass spectrum was recorded on an AutoSpec Premier (Waters) instrument. FTIR spectra (KBr) were taken on a Nicolet iS10 apparatus. For UV-Vis measurements an UNICAM UV 300 series apparatus was used. Fluorescence spectra were recorded on a luminescence spectrometer (AMINCO Bowman Series 2 spectrofluorometer) using the flash xenon lamp. The bandpass of excitation and emission monochromators was 16 nm. Spectroscopic measurements were carried out in 1 cm quartz cuvettes in solvents of the highest available purity. The solution pH was measured by an pH-meter CPC-511 with glass electrode EPS-1 (ELMETRON), standardized with buffer solutions. Portable LED light box (23 × 23 × 23 cm) was used to guarantee the reproducibility of the photos (PULUZ, Photography Light Box, Shenzhen Puluz Technology Limited). Pictures were taken by a Smartphone LG K10.

2.3. Synthesis of L

Compound **L** was obtained by diazocoupling reaction of diazonium salt with pyrrole, giving the product as orange solid with satisfactory 73 % yield. The procedure of the synthesis and structural characterization of **L** in given in Supplementary Material.

2.4. Lipophilicity (logP)

The lipophilicity values (logP$_{TLC}$) of ligand was estimated by TLC method using reverse phase chromatography (RP18) with a mixture of methanol:water (9:1, v/v) as mobile phase. As standards BBPA, NPOE, DOS, DOP and DBP were used. On the basis of comparison of R$_f$ values for standards and ligand logP$_{TLC}$ values was determined [63-65].

2.5. X-ray structure

Diffraction intensity data for **L** were collected on an IPDS 2T dual beam diffractometer (STOE & Cie GmbH, Darmstadt, Germany) at 120.0(2) K with MoKa radiation of a microfocus X-ray source (GeniX 3D Mo High Flux, Xenocs, Sassenage, 50 kV, 1.0 mA, and λ = 0.71069 Å). Investigated crystals were thermostated under a nitrogen stream at 120 K using the

5

CryoStream-800 device (Oxford CryoSystem, UK) during the entire experiment. Data collection and data reduction were controlled by using the X-Area 1.75 program (STOE, 2015). Due to low absorption coefficient no absorption correction was performed. The structure was solved using intrinsic phasing implemented in SHELXT and refined anisotropically using the program packages Olex2 [66] and SHELX-2015 [67]. Positions of the C–H hydrogen atoms were calculated geometrically taking into account isotropic temperature factors. All hydrocarbonic H-atoms were refined as riding on their parent atoms with the usual restraints. Both OH and NH atoms were found in the Fourier electron density map and refined without constraines. Structure of **L** was refined with no special treatment.

2.6. Complexation studies

Metal cation complexation studies were carried out using UV-Vis titration in acetonitrile, dichloromethane, methanol, DMSO and the mixture of DMSO with water. A series of solutions of pH values ranging from 2 to 12 was prepared by mixing sodium hydroxide solution (0.1 M) and hydrochloric acid (0.1 M). Simulated body fluid (SBF), phosphate buffer saline (PBS) and artificial urine (AU) samples were prepared according described procedures [68-70]. The stock solutions of **L** ($\sim 10^{-3}$ M), metal perchlorates ($\sim 10^{-2}$ M), TsOH ($\sim 10^{-2}$ M), TBAOH ($\sim 10^{-2}$ M) and chlorides ($\sim 10^{-2}$ M), were prepared by weighting the respective quantities of them and dissolving in the respective solvent system in volumetric flasks. The values of binding constant (logK) were calculated with the use of OPIUM [71] program on the basis of titration experiment data. Limits of detection (LOD) for copper(II) were calculated DL $= 3\sigma/k$, where σ is the standard deviation of the blank and k is the slope of the linear function A = f(molar concentration of analyte). The spectral response towards copper(II) was expressed as $\Delta A = A_{Cu} - A_0$, where A_0 stands for absorbance of solution of **L** (or optode) and A_{Cu} absorbance value of **L** (or optode) in the presence of copper(II) salt. The influence of interfering ions on spectrophotometric response towards copper(II) was expressed as the absolute value of relative response RR% = $|[(A - A_{Cu})/A_{Cu}]|\times 100\%$, where A_{Cu} stands for absorbance of solution of **L** in the presence of copper(II) chloride (equimolar to ligand amount) and A is absorbance value measured just after addition of interfering metal chloride in the same quantity, 10-fold and 100-fold molar excess in relation to copper(II) chloride [65, 72].

2. 7. Digital color analysis

Pictures were analyzed using free software ImageJ [73, 74]. The change of optode color given as ΔE_{RGB} [75] was calculated using the equation: $\Delta E_{RGB} = [(R_0 - R)^2 + (G_0 - G)^2 + (B_0 - B)^2]^{1/2}$ where R_0, G_0 and B_0 values correspond to color of solution (or optode) in the absence of

6

copper(II) salt, and R, G and B values correspond to color of solution (or optode) in the presence of copper(II). The value of the intensity of green color I_G was calculated using the equation: $I_G = -\log(G/G_0)$.

2.8. Test Strips

Solutions of **L** (~10^{-3} M or ~10^{-4} M) in dichloromethane were poured into a chromatographic chamber, into which a strip of glass microfiber filter or filter paper was placed. After 5 min. strips were taken out and solvent was evaporated in a stream of hot air.

2.9. Cotton swabs

Cotton swabs [76] were soaked with the 100.0 μL of **L** solution (~10^{-3} M or ~10^{-4} M) in dichloromethane and left for solvent evaporation.

2.10. Membrane preparation

CTA optodes were prepared according to previously described procedures [72]. Membranes contained 250.0 mg of CTA, 1.0 mg of **L**, 168.6 mg (150.0 μL) of TEG and 0.5 mg of KTClPB. All components of optodes were dissolved in dichloromethane (6 mL) with continuous stirring using a magnetic stirrer for 2 h and were sonicated for ca. 15 min. – until a clear solution is formed. In the next step, solutions were poured on, prepared in advance (washed with nitric acid, deionized water, acetone and 2-propanol) Petri dish (9 cm diameter), covered loosely with a lid and left for solvent evaporation. After 24 h obtained optode films were peeled off from the Petri dish and cut into 0.9×4.5 cm strips. Blank membranes were prepared in an analogous way using all components besides chromoionophore **L**.

3. Results and discussion

3.1. Synthesis and characterization of *L*

New compound **L** was obtained with satisfactory yield (73%) in a simple diazocoupling reaction of diazonium salt (1a) of 4-amino-4-nitrophenol (1) with pyrrole (2) in aqueous solution of pH ~ 10 (NaOH) (Fig. 1). Crystallization from dichloromethane preceded by column chromatography isolation gave a pure compound in the form of long orange needles. Spectral data (^{1}H and ^{13}C NMR, HRMS and IR) confirming the structure of newly obtained azopyrrole dye **L** are included in Supplementary Information (Fig. S1). As an additional parameter characterizing new compound **L** its lipophilicity logP 3.40±0.02 was determined using TLC method.
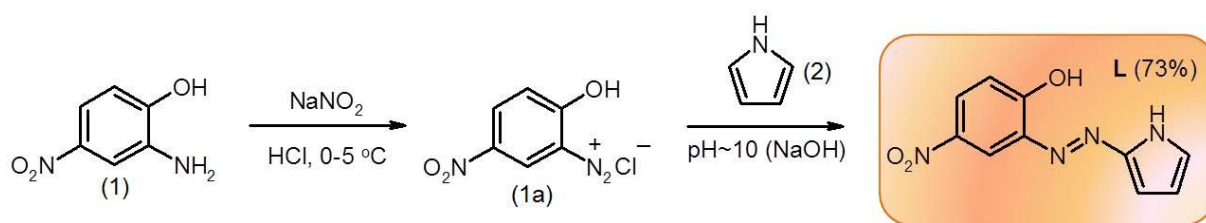
Fig. 1. Synthetic route for **L**.

3.2. Structure of *L* in solution

Hydroxyazocompounds are known to undergo prototropic tautomerism resulting in azophenol ⇄ quinone-hydrazone equilibrium [77-79]. Tautomeric equilibrium depends on several factors, both structural (e.g. type and location of substituents, macrocyclic/acyclic structure) and those resulting from the chemical environment of molecule like solvent and its properties, the presence of ionic species [80-83]. From the other hand, azo compounds bearing pyrrole moiety can be also considered as systems of possible prototropic tautomeric equilibrium proceeding with the engagement of N-H pyrrole proton [84]. Taking all of this into account for investigated here **L** tautomeric equilibrium shown in Fig. 2 can be considered.
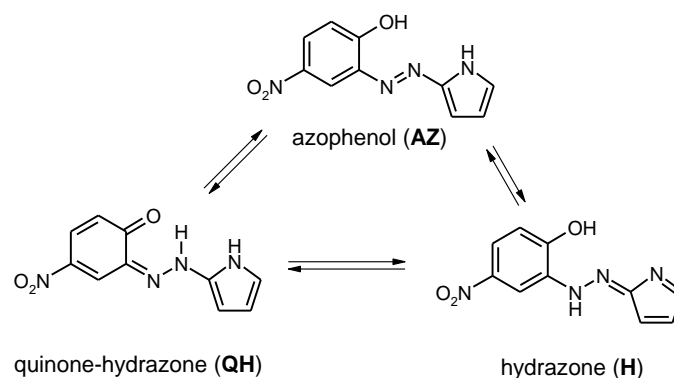

Fig. 2. Proposed tautomeric equilibrium of **L**.

Tautomeric equilibrium of **L** was investigated in solution using NMR spectroscopy. ^{1}H NMR spectra were registered in acetonitrile-d_3, DMSO-d_6, methanol-d_4 (Fig. 3). Signals of protons of pyrrole moiety are observable as multiplets at ∼ 6.5, 7.1 and 7.4 ppm. Signals of benzene protons are seen as well shaped signals characteristic for 1,2,4-substituted benzene at ∼8.5 (d, J ∼ 2 Hz), 8.2 (dd, J1 ∼ 2 Hz, J ∼ 9 Hz) and doublet 7.3 (d, J ∼ 9 Hz). Signals of protons of OH and NH groups seen as singlets at above 10.0 ppm (acetonitrile-d_3, DMSO-d_6) provide the evidence for hydrogen bonded system. Comparing with acetonitrile, in highly dipolar DMSO stronger hydrogen bonding between solvent acting as proton acceptor and **L** as hydrogen bond donor is expected, which correlates with the observed position of N$\underline{H}$ and O$\underline{H}$ proton signals at 10.93 and 11.92 ppm respectively. Signals of aromatic protons are shielded

8

comparing to acetontrile. Analyzing the observed spectral pattern in ^{1}H NMR spectra it can be concluded that in all investigated solvents **L** exists in azophenol (AZ) form.
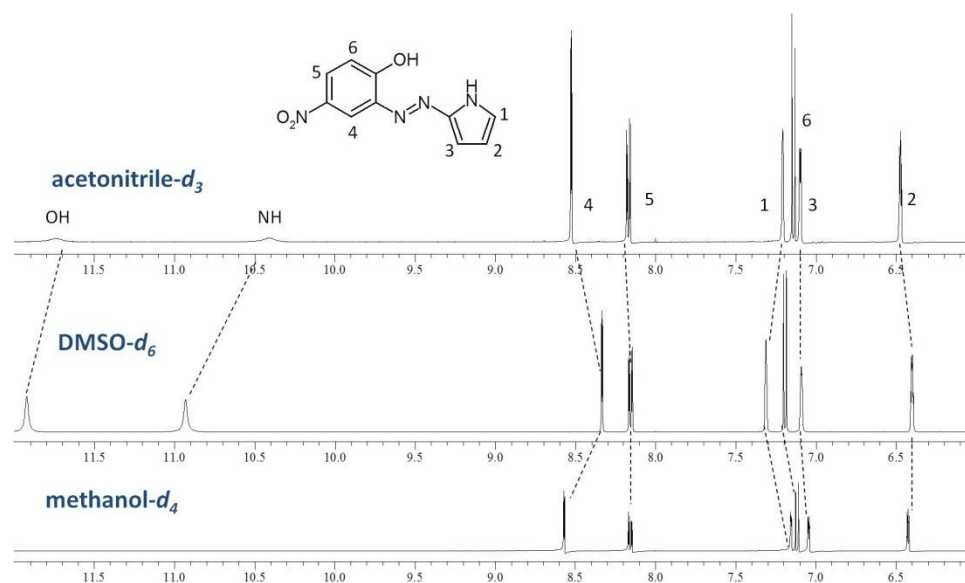

Fig. 3. ^{1}H NMR spectra of **L** in various solvents.

UV-Vis spectra of **L**, where lower than in NMR experiments concentrations of solute are used, were also registered in different solvents (Fig. 4(a)). In all cases, namely acetonitrile, DMSO, methanol and dichloromethane two absorption bands are observed in spectrum of **L**. The first one, of lower value of molar absorption coefficient, at ~ 310 nm and the second one of higher intensity at ~ 420 nm in acetonitrile and dichloromethane. The last mentioned absorption band in methanol is broaden and right side asymmetric. In DMSO, broader than in acetonitrile and dichloromethane absorption peak is additionally coming along with a band of low intensity on the red side of absorption, within 500 and 575 nm. The differences in spectral pattern in DMSO and methanol are manifested by deeper yellow color of solution of **L** in these solvents (Fig. 4(b)), what can suggest the solvation effect [85]. The relative intensity of band at ~520 nm in spectrum of **L** registered in DMSO depends on **L** concentration (Fig. 4(c)). Also the relative intensity of bands at 420 and 520 nm is concentration dependent and the value of the molar absorption coefficient (515 nm) is decreasing with the increase of the concentration (Fig. 4(d)). It can be associated with the presence of various forms of dye or can be an effect of dye-dye interactions in solution - self-organization. UV-Vis spectroscopy is one of the useful tools for investigation of aggregation process [86] and as it is reported by other authors the spectral pattern observed in case of **L** might point out the formation of different types of aggregates [87, 88]. Moreover, in fluorescence spectra of solutions of **L** of the same concentrations in above mentioned solvents emission bands are detectable in dichloromethane, acetonitrile and methanol (Fig. 4(e)). In DMSO under the same measurement conditions

9

fluorescence is too weak to register emission spectrum. It can be connected with well-known aggregation-caused quenching (ACQ) effect due to π-π stacking interactions. Such interactions for **L** were confirmed in solid state (*vide infra*).
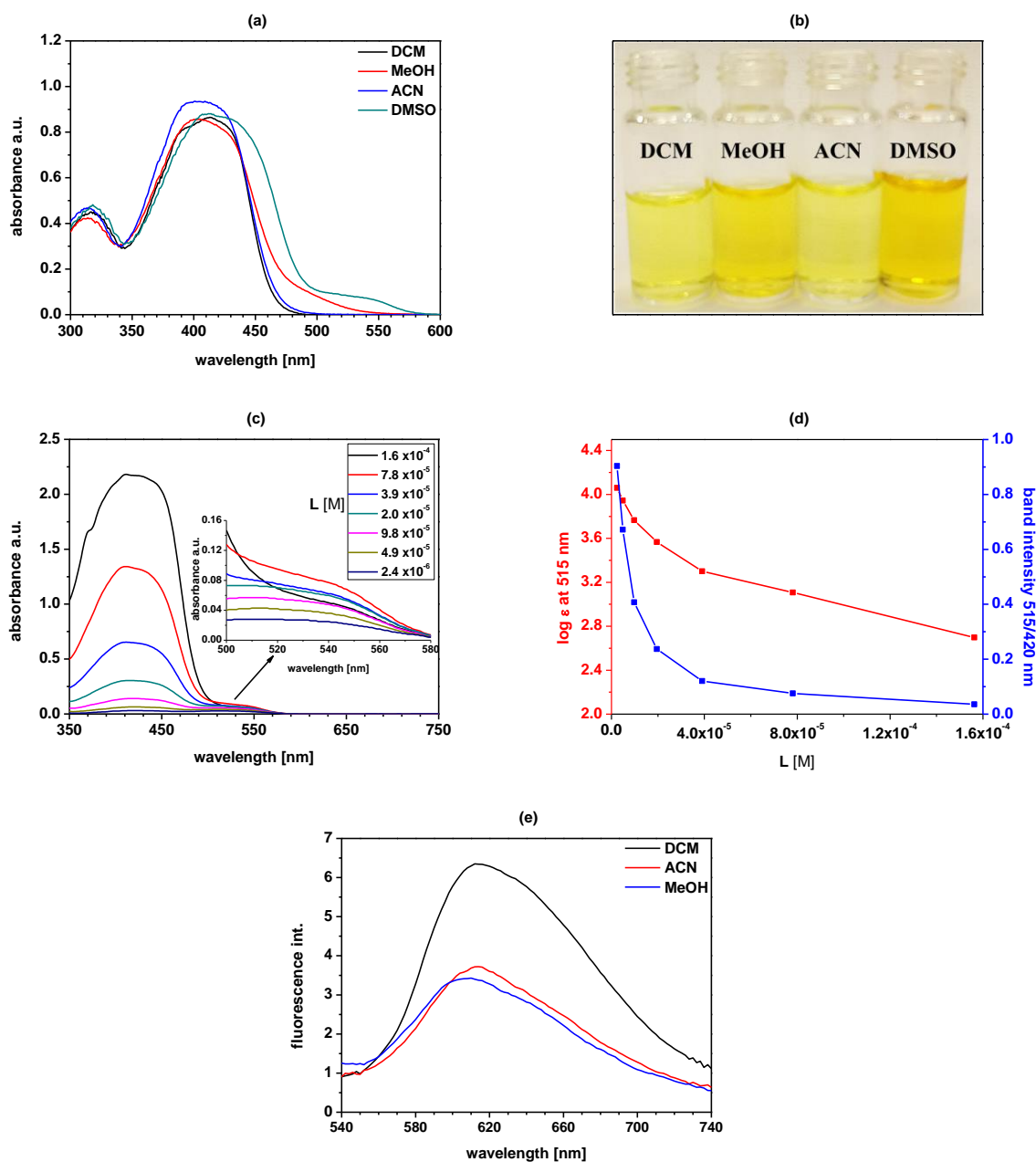

Fig. 4. (a) UV-Vis absorption spectra of **L** ($4.05×10^{-5}$ M) in different solvents; (b) Solutions of **L** ($1.02×10^{-4}$ M) in different solvents; (c) UV-Vis absorption spectra registered for solutions of different concentration of **L** in DMSO; (d) Correlation of relative intensity of bands and the molar absorption coefficient with the concentration of **L** in DMSO; (e) Emission spectra of **L** ($1.02×10^{-4}$ M) registered in different solvents (λ_{ex} 600 nm, λ_{em} 618 (dichloromethane - DCM); 614 (acetonitrile - ACN and methanol - MeOH).

3.3. Structure of **L** in solid state

Single crystals of **L** suitable for X-ray analysis were obtained by crystallization from dichloromethane. Molecular view of **L** is shown in Fig. 5. Crystal data and structure refinement details are collected in Table 1. Compound **L** forms needle, red crystals, with symmetry of the monoclinic system, the space group $P2_1/n$ (no. 14). Asymmetric unit contains one molecule and the whole unit cell is built from four molecules, Z = 4. Most of the bond lengths and angles are in the expected ranges (see Fig. 5). Based on short interatomic distances one may assume mostly double character of N1-N2 bonds and aromatic character of the pyrrolic ring. The molecule is essentially flat. Dihedral angle between the phenyl ring and NO_2 group plane is ca -5°. Hydroxyl group forms internal H-bond with N2 atom, while the N-H hydrogen bond donor forms intermolecular interaction with O2 atom from neighbor molecule nitro group (Fig. 6, left). For details, see Table 2.
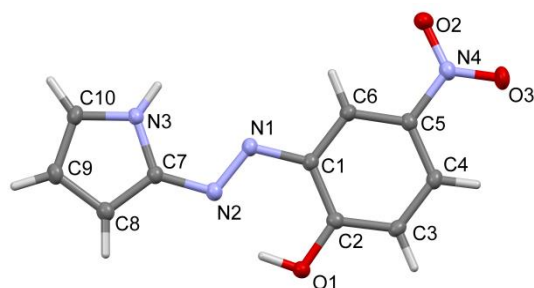

Fig.5. Molecular view of **L** showing atom labeling scheme. Displacement ellipsoids drawn at 50% probability level. Selected bond lengths (Å) and angles (°): N1-N21.2842(13), N1-C1 1.4033(13), N2-C7 1.3722(13), N3-C7 1.3738(14), C2-O1 1.3433(13), N4-O2 1.2340(13), N4-O3 1.2276(12), N4-C5 1.4547(14); valence angles: N2-N1-C1 115.55(9), N1-N2-C7 113.24(9), C10-N3-C7 108.79(9), O3-N4-O2 122.90(10), O1-C2-C1 122.16(9); torsions O3-N4-C5-C4 -5.5(2), O2-N4 C5 C6 -4.8(2) C2-C1-N1-N2 0.0(2).

Table 1. Crystal data and structure refinement details for **L**

	L
CCDC no.	2190550
Empirical formula	$C_{10}H_8N_4O_3$
M_r/g mol^{-1}	232.20
Temperature/K	120 K
Crystal system	Monoclinic
Space group (IT No.)	$P2_1/n$ (14)
a/Å	11.6673 (15)
b/Å	3.7411 (5)
c/Å	22.581 (3)
α/°	90
β/°	92.829(11)
γ/°	90
Volume/Å^3	984.4 (2)
Z	4
ρ_{calc} g/cm^3	1.567
Crystal size/mm^3	0.52 × 0.12 × 0.05
Radiation	Mo Kα (λ = 0.71073)
2Θ range for data collection/°	3.2–58.4
Reflections collected/unique	8887/2631

11

Completeness to θ_{max} (%)	99.8
Data/restraints/parameters	3631/0/162
Goodness-of-fit on F^2	1.07
Final R indexes [I>=2σ (I)]	$R_1 = 0.0398$, $wR_2 = 0.1121$
Final R indexes [all data]	$R_1 = 0.0463$, $wR_2 = 0.1164$
Largest diff. peak/hole / e Å^{-3}	0.37/ -0.23

Table 2. Hydrogen-bond geometry (Å, º) for **L**

D—H$\cdots A$	D—H	H$\cdots A$	$D\cdots A$	D—H$\cdots A$
N3—H3$\cdots$O2^i	0.859 (19)	2.142 (19)	2.9988 (13)	175.2 (17)
O1—H1$\cdots$N1	0.93 (2)	2.45 (2)	2.9635 (13)	114.9 (15)
O1—H1$\cdots$N2	0.93 (2)	1.79 (2)	2.6121 (13)	145.3 (18)

Symmetry code: (i) $-x+1$, $-y$, $-z+1$.

Crystal packing (Fig. 6) is dictated by hydrogen bonding and stacking interactions between the aromatic rings of the same nature. Actually the centroid distance between both planes, 3.741(8) Å, is equal to the *b* parameter of the unit cell, and is a pure lattice translation, so the dihedral angle between the planes α is equal to zero.
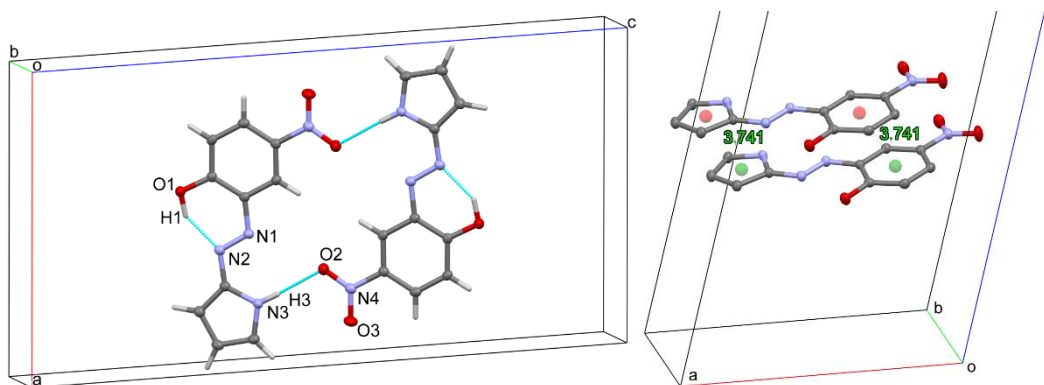

Fig. 6. Left: Hydrogen bonding in compound **L**, selected atom labels shown, cyan dashed lines show direction of bonding. Both molecules are related by the inversion centre at (½ 0 ½). Right: Stacking interactions in **L**. Centroids for pyrrole rings and phenyl rings have equal distance of one another (3.741(9) and 3.741(8) Å for pyrrolic and phenyl rings, respectively).

3.4. Acid-base properties of *L*

Azocompounds - weak bases - are protonated at one of two azo N-atoms forming non symmetric π-complex [89]. Protonation of azobenzenes usually leads to red shift of absorption band observed as a significant color change. However, the introduction of heterocyclic moiety instead of one of benzene ring can significantly change the properties of azocompound including acid-base properties [46]. In case of **L**, ionization of molecule can be also an effect of the deprotonation of hydroxy group, which typically for ionized dye molecules causes the color change resulting from the appearance of the red shifted absorption band of deionized form.

12

Quantitative colorimetric probes of the acid-base properties of **L** in different solvents are shown in Fig. 7 (top). The presence of *p*-toluenesulfonic acid (TsOH) slightly influences the color of the solutions what is in agreement with very small changes in absorption spectra. Titration trace of **L** with TsOH in methanol and DMSO is exemplified in Fig. 7(a) and (b).
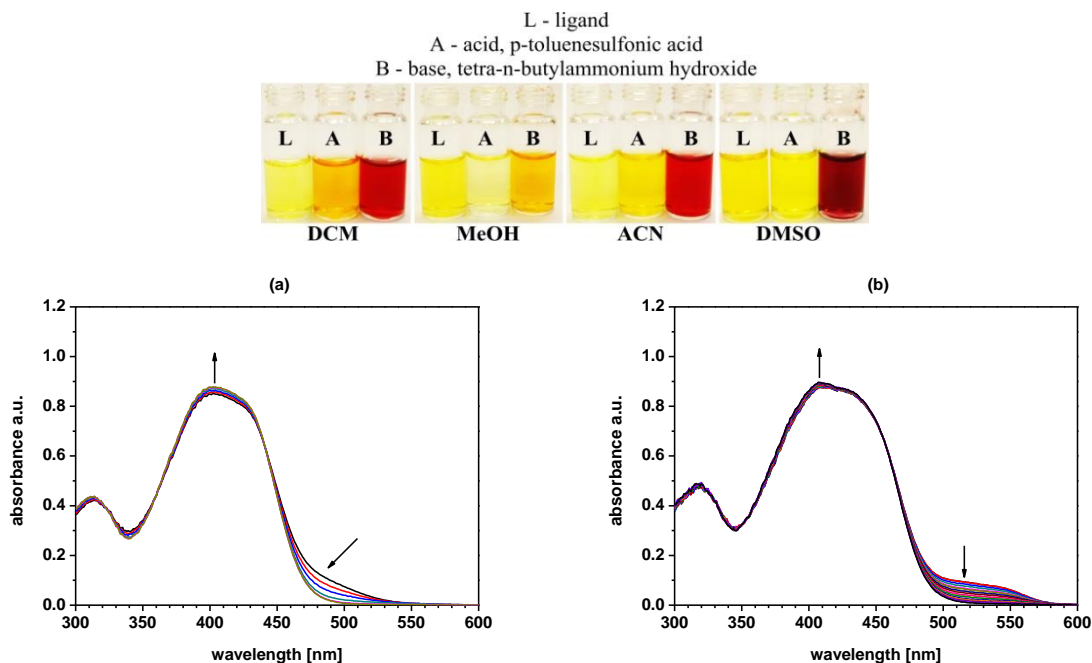

Fig. 7. Top: solutions of **L** (1.02×10^{-4} M) in different solvents with acid or base. Bottom: spectral changes upon titration of **L** ($c_L = 4.05 \times 10^{-5}$ M) with TsOH in (a) methanol (c_{TsOH} = 0-2.03×10^{-5} M) and (b) DMSO (c_{TsOH} = 0-2.05×10^{-5} M).

Upon titration with TsOH the only observed change in UV-Vis spectra is the decrease of the band in a region of 500-575 nm. This can support the thesis drawn above as this band comes from the dye-dye interactions in solution. The presence of acid can destroy the hydrogen bonded self-organized structure of **L** in solution (UV-Vis titration in dichloromethane was not carried out due to low solubility of TsOH in this solvent). This is evidenced in ^{1}H NMR spectra (Fig. 8) registered for **L** in the presence of equimolar and 5-fold excess of TsOH. The most significant change in spectra is the broadening and lowering of the intensity and finally the disappearance of the N-H proton signal at 10.93 ppm. Signals of protons of benzene rings are not changed both in the position and shape (for full range spectra and the values of chemical shift see Fig. S2 and Table S1), whereas signals of protons of pyrrole ring are slightly shielded and changed in shape. It means that N-H proton also in solution (similarly as in a solid state) can be engaged in the formation of hydrogen bond, probably intermolecular H-bonding with the nitro group of neighboring molecule of **L**.
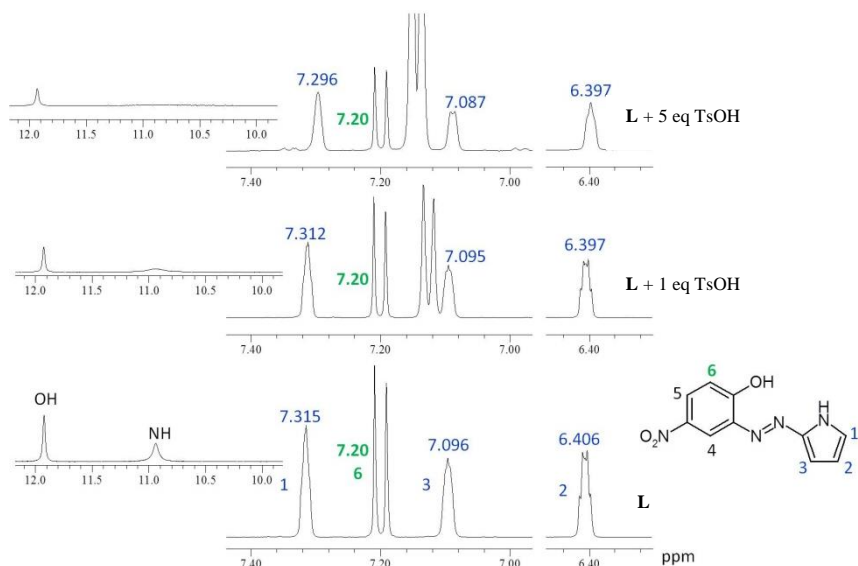
Fig. 8. Partial ^{1}H NMR spectra of **L** 1.42×10^{-2} M (bottom), **L** in the presence of equimolar (middle) and 5-fold excess (top) of TsOH in DMSO-d_6.

Titration of **L** with tetra-n-butylammonium hydroxide (TBAOH) results with the appearance of new bathochromically shifted absorption band with maxima at 468, 502 and 512 nm in methanol, acetonitrile and DMSO respectively (Fig. 9(a)-(c)). The values of equilibrium constants logK (**L**:TBAOH, 1:1) are comparable in methanol and acetonitrile 4.45±0.01 and 4.59±0.03, whereas the higher value was obtained in DMSO 5.45±0.03. The logK values correlate with the value of the spectral shift between bands of neutral and ionized form in absorption spectra: the largest in DMSO, and the lowest in methanol (Fig. 9(d)).
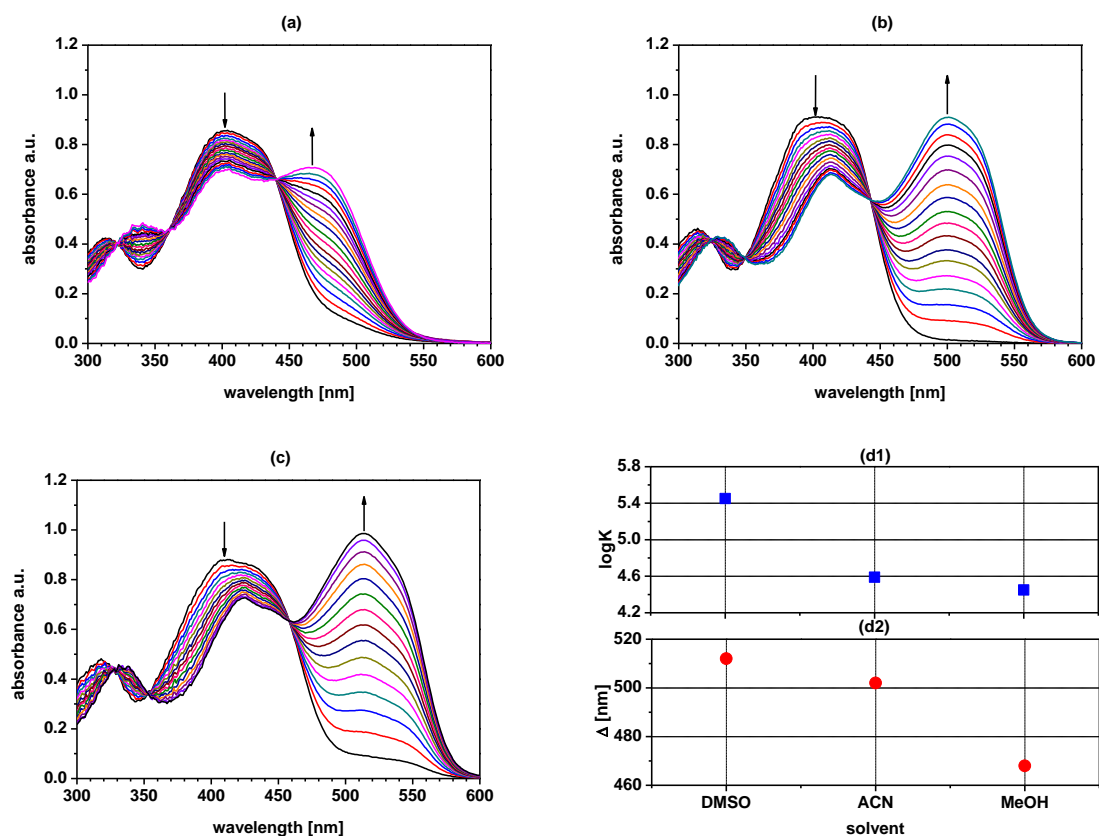
Fig.9. Spectral changes upon titration of **L** ($c_L = 4.05 \times 10^{-5}$ M) with TBAOH in (a) methanol ($c_{TBAOH} = 0\text{-}4.20 \times 10^{-5}$ M), (b) acetonitrile ($c_{TBAOH} = 0\text{-}8.26 \times 10^{-5}$ M) and (c) DMSO ($c_{TBAOH} = 0\text{-}4.34 \times 10^{-5}$ M). (d) The relationship between logK value and the spectral shift Δ [nm] in dependence of the type of solvent.

In the ^{1}H NMR spectrum of **L** registered in equimolar amount of TBAOH (DMSO-d_6) (Fig. S3) its deprotonation as one might expected is seen as disappearance of OH and NH proton signals and shielding of all signals of aromatic protons.

3.5. Complexation of metal cations in solution

The presence of azo moiety, with one of the nitrogen acting as a donor atom, in connection with the *o*-hydroxyl group and heterocyclic residue makes the structure of **L** similar to well-known metallochromic reagents. Metal cation complexation for **L** was investigated with the use of spectroscopic methods.

Quantitative colorimetric probes of metal cation complexation, realized in practice as an addition of the excess of metal perchlorate to solution of **L** (Fig. 10(a)), showed that the most significant, specific color change from yellow to purple is observed only for copper(II) perchlorate in methanol and DMSO. Some changes in color of the solution of **L** in methanol and DMSO are observed also in the presence of the excess of nickel(II), zinc(II) and lead(II) perchlorates. The excess of these salts, added to solutions of **L** as solid salts, cause the formation of the spectral bands falling in a spectral region of copper(II) complex absorption (Fig. S4). It

15

means that these salts in extremely high concentrations can influence the detection and determination of copper(II).

The change of color in the presence of copper(II) perchlorate is a result of the formation of new absorption bands at 540 and 556 nm respectively in UV-Vis spectra (Fig. 10(b) and (c)). The values of stability constants logK 5.21±0.02 (methanol) and 5.42±0.06 (DMSO) of 1:1 complexes (Job's plots) were calculated from titration data using OPIUM software. The titration trace and Job's plots (insets) in methanol and DMSO are shown in Fig. 10(b) and (c). The presence of metal perchlorates does not affect the color of solution in dichloromethane.
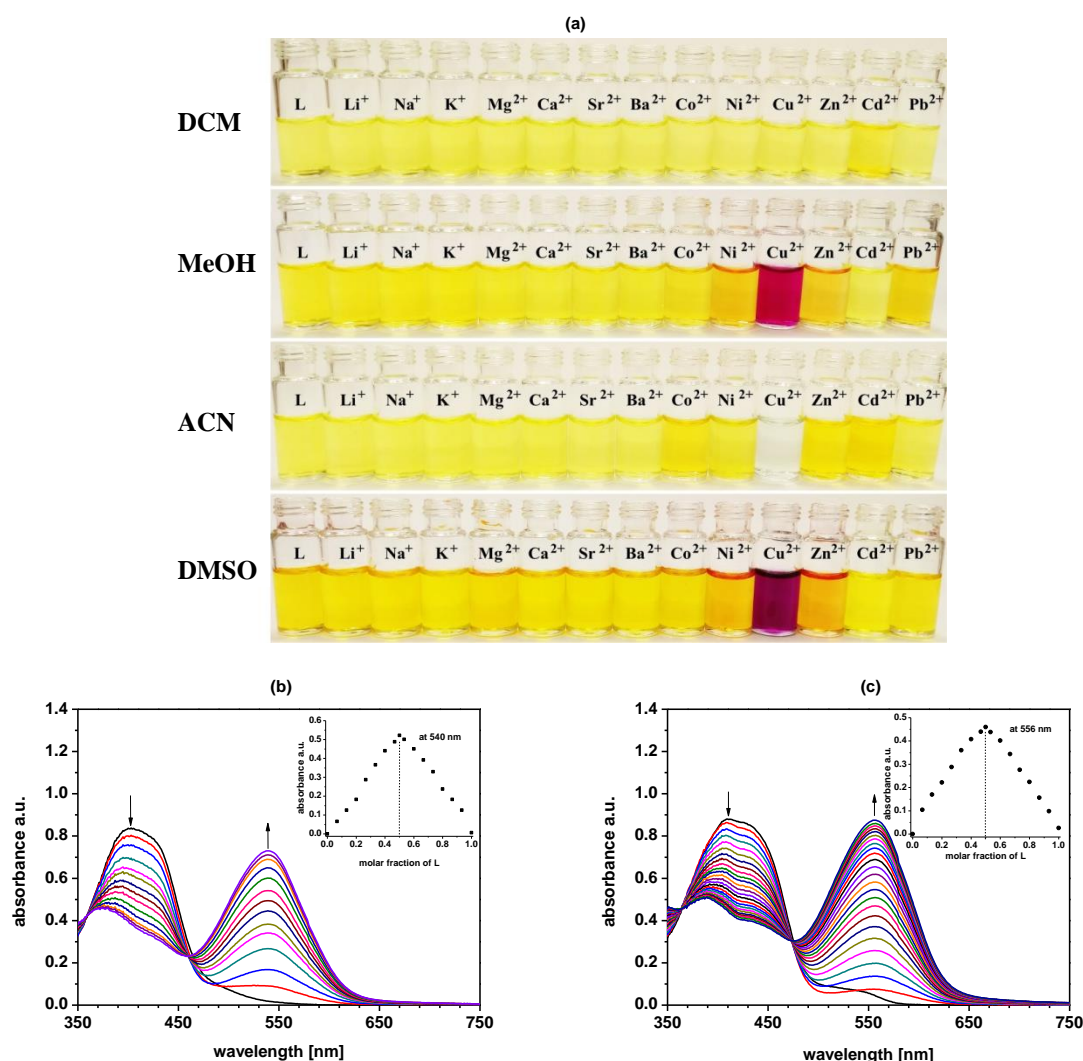

Fig. 10. (a) The change of the color of **L** ($c_L = 1.02 \times 10^{-4}$ M) in the presence of the excess of metal perchlorates in various solvents; from the top: dichloromethane (DCM), methanol (MeOH), acetonitrile (ACN) and DMSO; changes in UV-Vis absorption spectra of **L** ($c_L = 4.05 \times 10^{-5}$ M) upon titration with copper(II) perchlorate in (b) methanol ($c_{Cu} = 0\text{-}1.19 \times 10^{-4}$ M) and (c) DMSO ($c_{Cu} = 0\text{-}8.26 \times 10^{-5}$ M). Insets: Job's plots.

Complex formation is probably connected with the change of the arrangement of the hydrogen bonding system in solution (at the beginning of titration experiment in methanol and

DMSO the intensity of absorption band in a region of 500-575 nm decreases upon addition of copper(II) perchlorate). Sharp isosbestic points at 460 nm and at 474 nm for methanol and DMSO providing the presence of two absorbing species under equilibrium are observed only upon addition of a certain amount of copper(II) salt (Fig. 11). ^{1}H NMR spectrum of **L** in the presence of 10-fold excess of copper(II) perchlorate was registered (having in mind paramagnetic properties of copper(II)). In the registered spectrum, as can be expected broad - all shielded - signals are observed (Fig. S5). The presence of OH and NH proton signals suggests that the interaction with copper(II) ions in DMSO does not cause deprotonation of the ligand. The upfield shift can point out the change of the hydrogen bonding system upon copper(II) complexation [90].
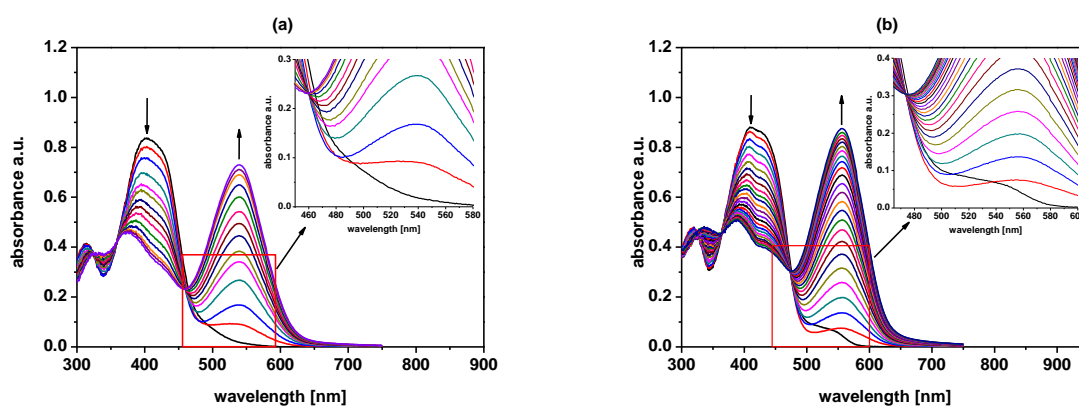

Fig. 11. UV-Vis titration trace of **L** ($c_L = 4.05 \times 10^{-5}$ M) for copper(II) perchlorate in (a) methanol ($c_{Cu} = 0$-1.19×10^{-4} M) and (b) DMSO ($c_{Cu} = 0$-8.26×10^{-5} M). Insets: spectral changes in region of isosbestic points and changes in a range 500-575 nm.

In acetonitrile at the beginning of titration the formation of a new, broad band at ~500 nm is observed. Higher amounts of copper(II) perchlorate causes the decrease of the absorbance in (Fig. S6) resulting in decolorization of solution. Due to possible side reactions of **L** with copper(II) perchlorate in acetonitrile this solvent was not considered for practical applications here. The nature of interactions of copper(II) - azo compounds (possible redox process) in acetonitrile is under investigation in our group.

From a practical, namely analytical point of view a selective response towards analyte in pure organic solvent has less importance than selective recognition in aqueous or mixed water-organic solvent systems. We found that the stability constant of the copper(II) complex of **L** has the highest value in DMSO. This hygroscopic solvent is well miscible with water and less toxic contrary to methanol. However saying that, the last studies have shown that DMSO is not so inert as it was considered for many years [91]. We carried out the spectrophotometric titration of **L** in mixed solvent system: DMSO with various water content (v/v) using in

17

experiments both copper(II) perchlorate (Fig. S7) and chloride (Fig. S8), as the last is one of the most ubiquitous anions in natural systems. In all mixed solvent system molar ratio plots shows 1:1 (**L**:Cu) stoichiometry of complex (Fig. S9 and S10).

The presence of a defined amount of water in a titrated system influences the value of spectral shift between free **L** and its copper(II) complex (color change is shown in Fig. S11), which is visualized schematically in Fig. 12(a). The largest value is observed in pure DMSO and systems with 10% of water, 144 nm. When water is present in 90% spectral shift is still over 100 nm, i.e. 122 nm (Fig. 12(b)). The benefit of the addition of water is the decrease of the intensity of the band of ligand in the region of 500-575 nm, where copper(II) complex absorbs. The counter ion has negligible effect on the difference between spectral shift of **L** and its copper(II) complex, however it affects the value of stability constant logK of copper(II) complex (1:1) (Fig. 12(c)). The stability constant values, at the same solvent composition, are higher when copper(II) chloride is used as a salt.
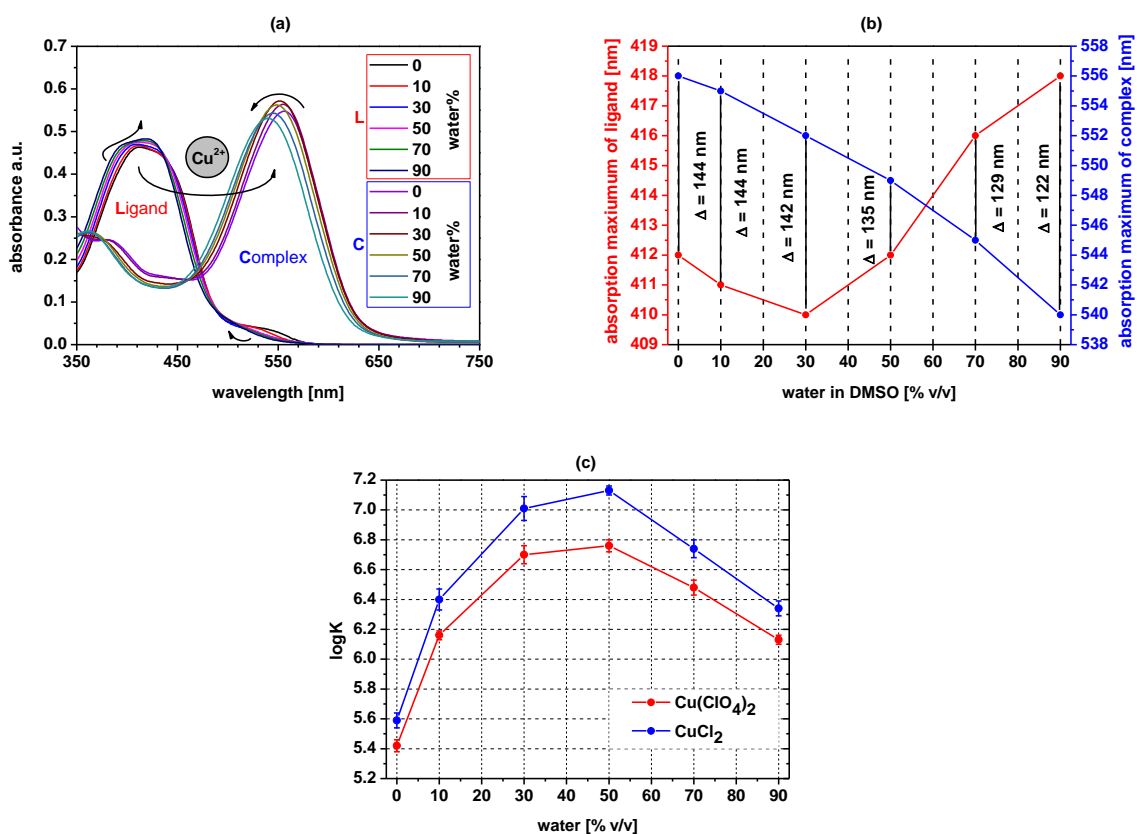
Fig. 12. (a) The influence of water content (%, v/v) in DMSO on spectral changes of **L** (2.16×10^{-5} M) and its copper(II) complex **C** (limiting spectra from copper(II) perchlorate titration experiments are shown); (b) the relationship between the position of the absorption maxima of **L** [nm] and its copper(II) complex [nm] and water content [%] in DMSO; (c) the comparison of the values of stability constants of copper(II) complexes (1:1) with **L** in dependence on counter ion.

Investigating the selectivity of colorimetric response of **L** towards metal cations (quantitative probes) it was found that color change of **L** from yellow to purple in solvent mixture water-DMSO (9:1) is observed only in the presence of copper(II) chloride (Fig.13). Slight changes of color to orange in the case of high concentrations of nickel(II) and lead(II) salts are observable and these ions may be considered as the main interfering ions.

Fig. 13. Color change of ligand ($c_L = 2.16 \times 10^{-5}$ M) in water-DMSO solution (9:1, v/v) in the presence of metal chlorides (pH 6.0).

3.6. Effect of pH

The effect of pH on spectral changes of **L** in water-DMSO (9:1, v/v) solution is shown in Fig. 14(a). With increasing pH the increase of absorption band at 470 nm is observed what can be connected with the deprotonation of **L**. It confirms the titration trace of **L** with sodium hydroxide (Fig. 14(b)) with clear isosbestic points suggesting two species under equilibrium. The spectral response ΔA towards copper(II) chloride (Fig. 14(c)) is constant in pH range 5.0-9.0 with linear response range $6.68 \times 10^{-8} – 1.67 \times 10^{-5}$M (Fig. 14(d)) and detection limit 5.00×10^{-8} M. Spectral changes upon titration of **L** with copper(II) chloride at pH 5.0, 7.0 and 9.0 in solvent mixture water-DMSO (9:1, v/v) are shown in Fig. S12. Only at pH 5 clear isosbestic point is observed, however it does not strongly influence the linear spectrophotometric response towards copper(II) presence (Fig. S13). Titration of **L** with copper(II) chloride in an alkaline environment (NaOH) gives linear response in a range of $6.68 \times 10^{-8} – 2.19 \times 10^{-5}$M (Fig. S14) and detection limit 6.19×10^{-8} M.
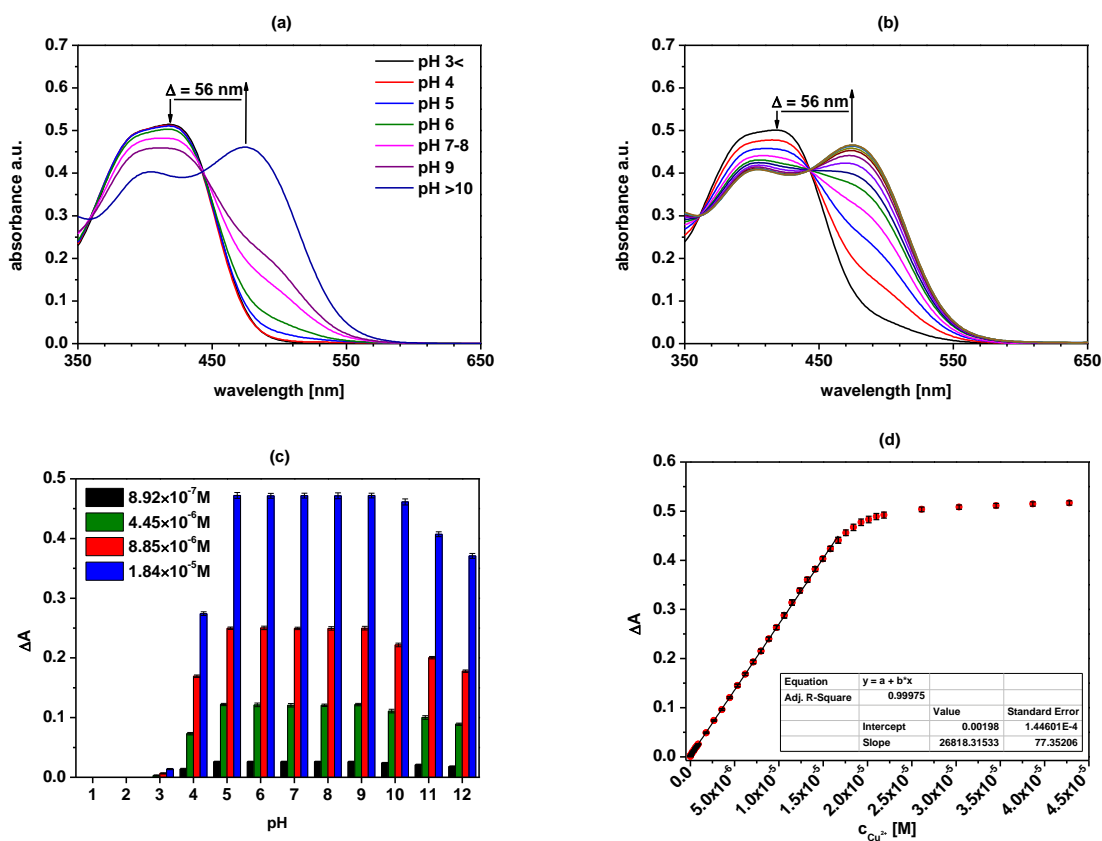
Fig. 14. The change of UV-Vis spectrum of **L** ($c_L = 2.16 \times 10^{-5}$ M) (a) with increasing pH and (b) upon titration with sodium hydroxide ($c_{NaOH} = 0\text{-}1.08 \times 10^{-5}$ M) in water-DMSO (9:1, v/v) from pH 6; (c) spectral response towards copper(II) chloride of **L** ($c_L = 2.16 \times 10^{-5}$ M) depending on pH ($\lambda = 540$ nm); (d) spectral response ΔA towards copper(II) chloride presence of **L** ($c_L = 2.16 \times 10^{-5}$ M) in pH range 5.0-9.0.

3.7. Regeneration

Regeneration cycles of **L** with 0.01 M EDTA solution after addition of copper(II) chloride are shown in Fig. S15. **L** can be regenerated at least 10 times without losing properties.

3.8. Interfering ions

The response of **L** was investigated in the presence of several interfering cations: Li^+, Na^+, K^+, NH_4^+, Mg^{2+}, Ca^{2+}, Sr^{2+}, Ca^{2+}, Ba^{2+}, Mn^{2+}, Co^{2+}, Ni^{2+}, Zn^{2+}, Cd^{2+}, Pb^{2+} and their mixture. Fig. 15 shows the influence of addition of equimolar, 10-fold and 100-fold molar excess of interfering metal chlorides on the spectrophotometric response of **L** at equimolar (to **L**) amounts of copper(II) chloride. The effect of interfering ions is given as RR% value, in water-DMSO (9:1, v/v) solvent mixture at pH 7.0. RR% value does not exceed 5% even in 100-fold molar excess of interfering ions and their mixture.
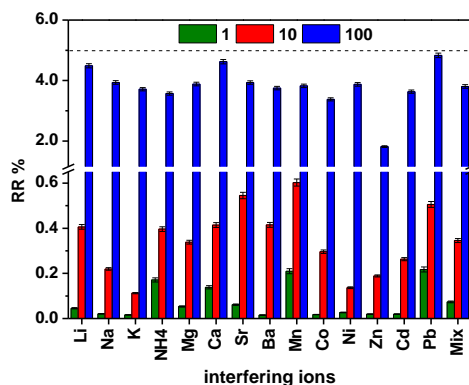
Fig. 15. Interferences of several metal chlorides used in equimolar, 10-fold and 100-fold molar excess, on the spectrophotometric response of **L** ($c_L = 2.16 \times 10^{-5}$ M) (540 nm) at equimolar (to **L**) amount of copper(II) chloride in water-DMSO (9:1, v/v) solvent mixture, pH 7.0.

3.9. Studies in multi-component solutions

The possibility of application of **L** for the detection of copper(II) was checked in mixtures of DMSO with multicomponent aqueous solutions, namely artificial urine (AU), simulated body fluid (SBF) and phosphate buffer saline (PBS) (9:1,v/v). Spectral changes upon titration of **L** with copper(II) chloride in AU (pH 6.0), SBF (pH 7.4) and PBS (pH 7.4) are shown in Fig. 16. In multi-component solutions the presence of ionic species significantly affects the spectral properties of **L**, which is manifested by the presence of two absorption bands at 405 and 474 nm in UV-Vis spectrum, but it does not significantly affect the range of the linear response (Fig. 17) and the limits of detection (Table S2) for copper(II). The UV-Vis spectrum of **L** in AU and SBF indicates partial ligand deprotonation, while in PBS compound **L** is in deprotonated form. Stability constant values (logK) of copper(II) complexes (1:1) calculated in AU, SBF and PBS are 6.31±0.04, 6.32±0.02 and 6.40±0.05, respectively.
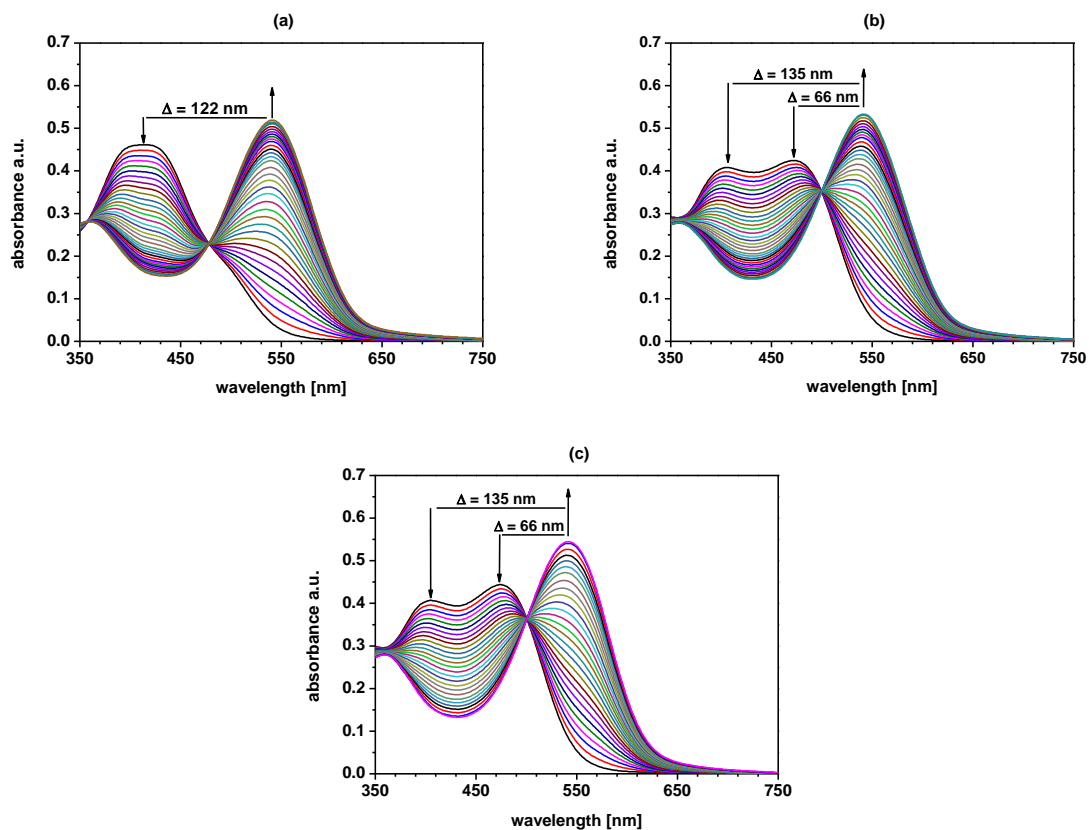
Fig. 16. The change of UV-Vis spectrum of **L** ($c_L = 2.16 \times 10^{-5}$ M) upon titration with copper(II) chloride ($c_{Cu} = 0$-4.28×10^{-5} M) in (9:1, v/v) solvent mixtures: (a) AU:DMSO (pH 6.0); (b) SBF:DMSO (pH 7.4) and (c) PBS: DMSO (pH 7.4).

Fig. 17. Linear responses of **L** ($c_L = 2.16\times10^{-5}$ M) upon titration with copper(II) chloride ($c_{Cu} = 0\text{-}4.28\times10^{-5}$ M) in (9:1, v/v) solvent mixtures: (a) AU:DMSO (pH 6.0); (b) SBF:DMSO (pH 7.4) and (c) PBS: DMSO (pH 7.4).

3.10. Digital color analysis

Fig. 18 shows color changes of **L** in solutions with increasing concentration of copper(II) chloride in solvents of different composition. Photos were taken using a Smartphone camera. Observable color changes, which can be traced by "the naked eye", were visible above the 10^{-7} M copper(II) chloride.

Fig. 18. Color changes of **L** ($c_L = 2.16\times10^{-5}$ M) upon titration with copper(II) chloride ($c_{Cu} = 0\text{-}4.28\times10^{-5}$ M) in water-DMSO (9:1, v/v) solvent mixture at pH: (a) 5.0; (b) 7.0; (c) 9.0 and (d) SBF:DMSO (9:1, v/v) at pH 7.4.

23

Using digital color analysis we combined different color dependences with concentration of copper(II) chloride. Fig. 19 shows these correlations in SBF:DMSO (9:1, v/v) solution. The largest range of the linear response $8.92 \times 10^{-7} - 2.18 \times 10^{-5}$ M was obtained for color ratio B/G with detection limit 1.07×10^{-7} M. However the lowest LOD = 8.66×10^{-8} M was obtained for color change ΔE_{RGB} with linear response $8.92 \times 10^{-7} - 1.32 \times 10^{-5}$ M. All color dependences with concentration of copper(II) chloride (Fig. S16-S19) at different pH are collected in Table S3.
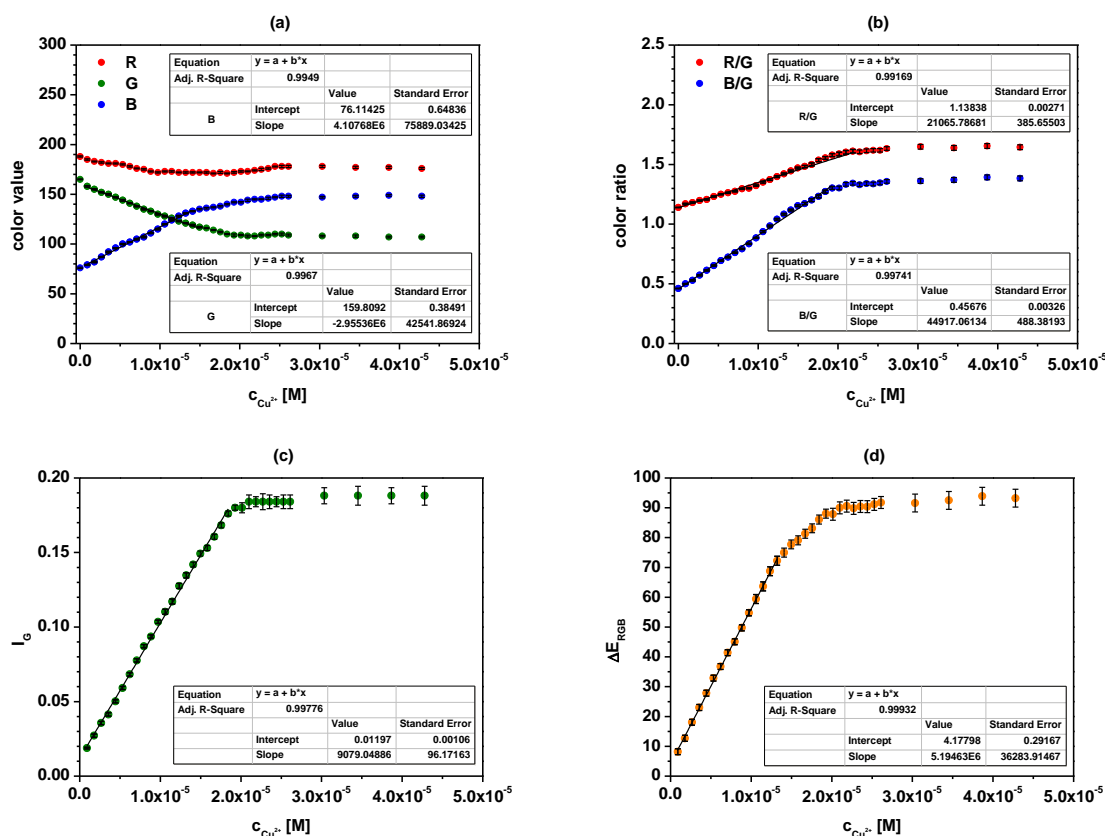
Fig. 19. Dependence of (a) color value, (b) color ratio (R/G, B/G), (c) color intensity (I_G) and (d) color change (ΔE_{RGB}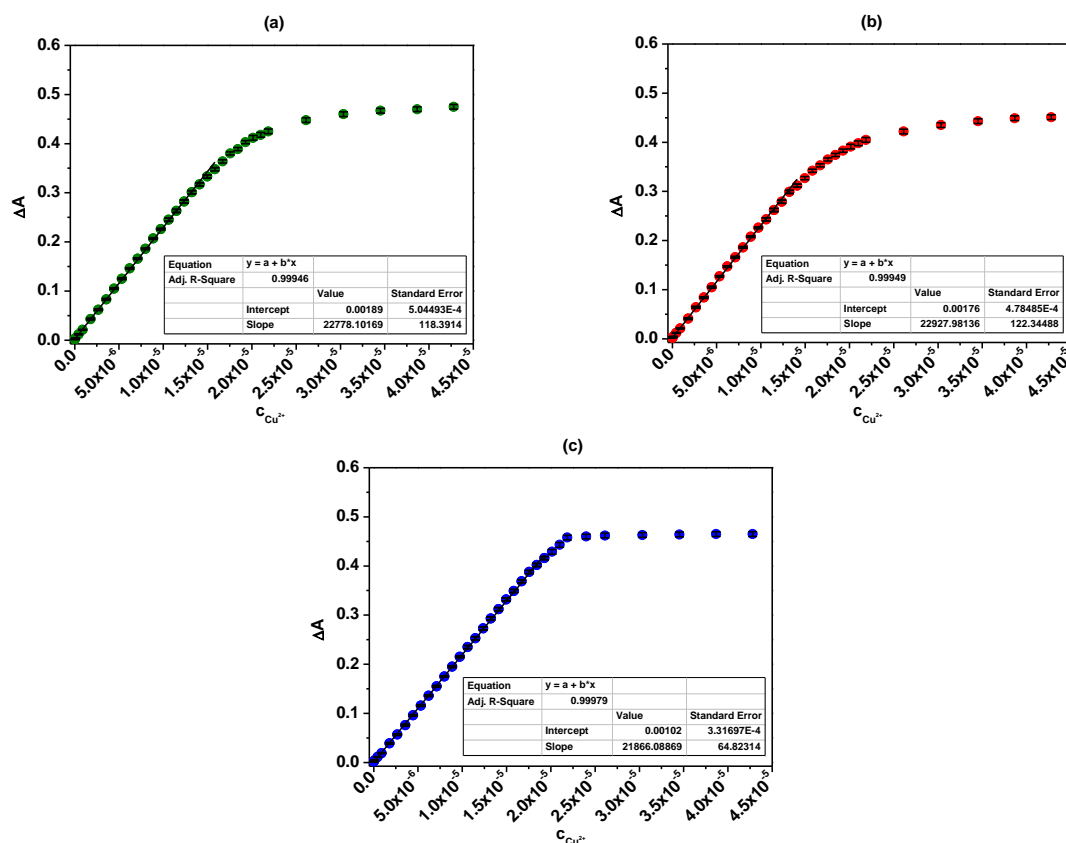) of **L** ($c_L = 2.16 \times 10^{-5}$ M) upon titration with copper(II) chloride ($c_{Cu} = 0\text{-}4.28 \times 10^{-5}$ M) in SBF:DMSO (9:1, v/v) at pH 7.4.

3.11. Comparison of chemosensor **L** with the other reported chemosensors.

In Table 3 we compared compound **L** with other reported chemosensors that use Smartphone camera detection for the determination of copper(II) [92-95]. The synthesized chemosensor **L** has many advantages over the other reported chemosensors such as: simple preparation, use of inexpensive reagents and lower detection limits than the other chemosensors.

Table 3. Comparison of chemosensor **L** with the other reported copper(II) chemosensors with Smartphone detection.

Chemosensor	Method	Medium	Linear response [M]	LOD [M]	Reference
Naphthalimide-based Schiff base	UV-Vis	DMSO	2.0×10^{-5} - 2.0×10^{-4}	1.60×10^{-6}	[92]
	Smartphone	EtOAc:H$_2$O (1:1, v/v, pH 4.8)	$0.0 – 1.0\times10^{-3}$	4.80×10^{-5}	
NBD[a]-benzimidazole based dyad	UV-Vis	MeOH:H$_2$O (1:1, v/v)	$0.0 - 1.5\times10^{-6}$	1.23×10^{-7}	[93]
	Smartphone	MeOH:H$_2$O (1:1, v/v)	5.0×10^{-7} - 3.5×10^{-6}	3.80×10^{-6}	
Red beet pigment	Smartphone	H$_2$O (pH 9.0)	4.0×10^{-6} - 2.0×10^{-5}	8.40×10^{-7}	[94]
Tri-imidazolium salt	Smartphone	DCM:DMSO (49:1, v/v)	$0.0 - 3.6\times10^{-5}$	5.10×10^{-7}	[95]
L	UV-Vis	H$_2$O:DMSO (9:1, v/v, pH 5.0-9.0)	$6.68\times10^{-8} – 1.67\times10^{-5}$	5.00×10^{-8}	This work
		SBF:DMSO (9:1, v/v, pH 7.4)	$6.68\times10^{-8} – 1.41\times10^{-5}$	5.85×10^{-8}	
	Smartphone	H$_2$O:DMSO (9:1, v/v, pH 5.0)	$8.92\times10^{-8} – 1.58\times10^{-5}$	8.33×10^{-8}	
		H$_2$O:DMSO (9:1, v/v, pH 7.0)	$8.92\times10^{-8} – 1.76\times10^{-5}$	7.72×10^{-8}	
		H$_2$O:DMSO (9:1, v/v, pH 9.0)	$8.92\times10^{-8} – 2.10\times10^{-5}$	6.37×10^{-8}	
		SBF:DMSO (9:1, v/v, pH 7.4)	$8.92\times10^{-8} – 1.32\times10^{-5}$	8.66×10^{-8}	

[a] 4-choloro-7-nitrobenzafuran

3.12. Tests strips and cotton swabs

Test strips and cotton swabs were used for fast and qualitative detection of copper(II) ions in water solutions. In Fig. 20 color changes of prepared sensors after immersion in solutions of different copper(II) chloride concentration are shown. Detection of copper(II) by naked-eye is possible above 1.0×10^{-5} M and 1.0×10^{-7} of copper(II) chloride for sensors where **L** was used in concentration of 1.04×10^{-3} M and 1.04×10^{-4} M, respectively.
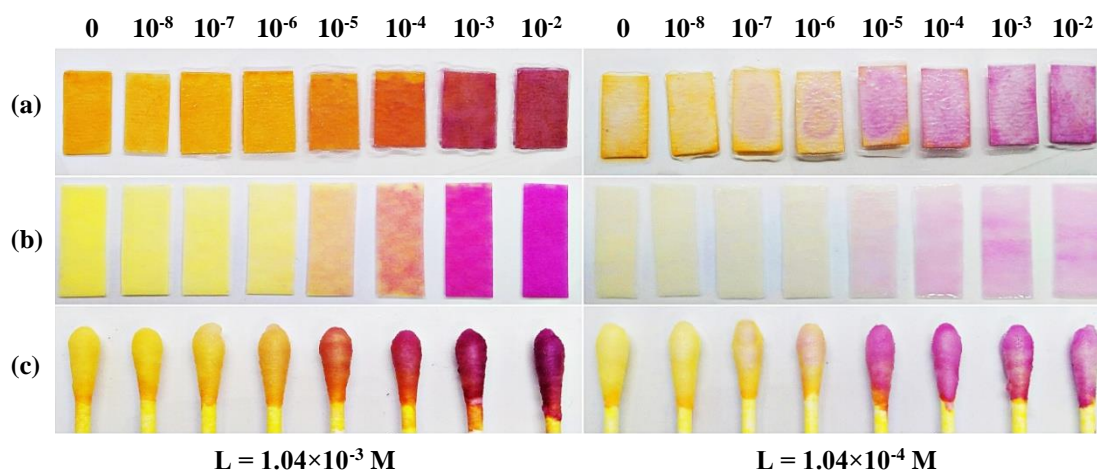
Fig.20. Color changes of test strips (a) glass microfiber filter and (b) filter paper; (c) cotton swabs.

3.13. Optodes

The response of cellulose triacetate (CTA) optode towards copper(II) was investigated spectrophotometrically (Fig. 21(a)). UV–Vis spectra of optodes before contact with copper(II) are similar to spectra of **L** registered in dichloromethane, acetonitrile and water-DMSO (9:1, v/v) below pH 5.0. The spectrophotometric response of optode in the presence of copper(II) chloride characterizes with the appearance of a new, bathochromically shifted absorption band,

which intensity increases with the increasing concentration of copper(II) chloride. The maximum of absorption of the optode based on **L** is located at 412 nm and is shifted towards 540 nm, when titrated with an aqueous solution of copper(II) chloride. It is consistent and comparable with spectral and color changes resulting from the formation of a complex of 1:1 stoichiometry, when titrating organic and water mixture solutions of **L** with copper(II) perchlorate and chloride. Thus it can be assumed that the observed spectral pattern for optodes can be a result of the complex formation between chromoionophore entrapped in a polymeric matrix and copper(II) chloride.

Linear response for optode with **L** (Fig. 21(b)) was found for copper(II) concentration range of $5.41 \times 10^{-8} - 2.48 \times 10^{-5}$ M with a regression equation of $\Delta A = 22769.9221 \times c_{Cu(II)} + 0.0011$ ($R^2 = 0.9971$) and detection limit 7.22×10^{-8} M. At concentration ca. 4.00×10^{-4} M sensor riches saturation with analyte.

To determine the response time, experiments using membranes immersed in two solutions of copper(II) chloride 1.0×10^{-5} M and 1.0×10^{-6} M, with contact time up to 15 min. were carried out. ΔA of the optodes as a function of time needed for reaching a constant optical signal is shown in Fig. S20. The optode was found to reach 95% of the final signal (t_{95}) within 2 min and 4 min for copper(II) concentration 1.0×10^{-5} M and 1.0×10^{-6} M, respectively.
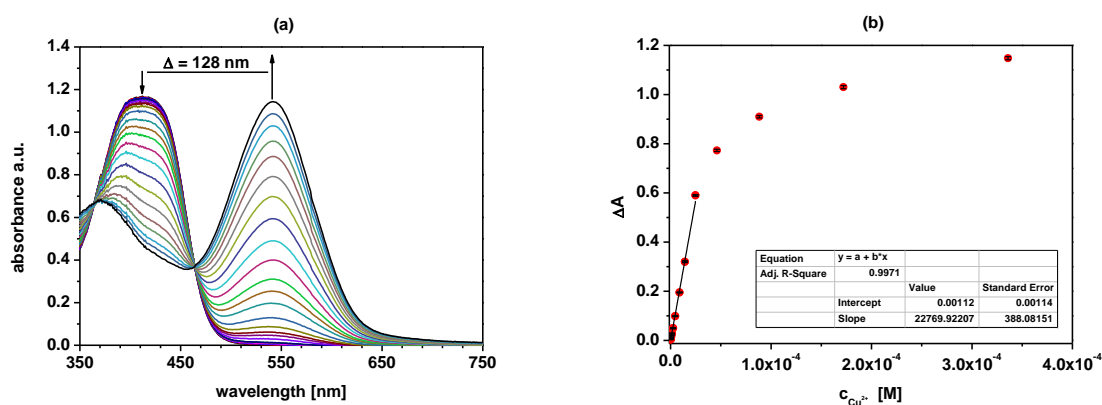
Fig. 21. (a) Changes in UV–Vis spectrum and (b) optical response of optode with **L** upon titration copper(II) chloride ($c_{Cu} = 0\text{-}3.36 \times 10^{-4}$ M) in aqueous solution (pH 5.0).

The reproducibility of optodes was evaluated by comparing the ΔA values of the copper(II) loaded membrane samples obtained in the different series for two concentrations 1.0×10^{-6} M and 1.0×10^{-5} M (Fig. 22(a)). The relative standard deviations for the measured ΔA values for 1.0×10^{-6} M and 1.0×10^{-5} M were 1.68% and 0.96%, respectively. The possibility of regeneration of optode after use - to make them reusable - was checked using a regeneration solution of 0.1 M HCl. Regeneration time for optode was less than 30 sec. After regeneration, optodes were washed three times with deionized water. In Fig. S21 regeneration of optodes is

26

shown after contact with 1.08×10^{-5} M copper(II) chloride solution. After ten cycles the drift of the optical signal was less than 1.27%. However in the same time some leaching of **L** from the polymer matrix was observed - the solution turned purple in color. This effect was investigated qualitatively using two concentrations of copper(II) salt chloride: 1.0×10^{-6} M and 1.0×10^{-5} M (Fig. S22). After ten cycles leaching of **L** from optodes for 1.0×10^{-6} M and 1.0×10^{-5} M were 12.9±0.1 and 29.4±0.3, respectively. Despite the leaching of the compound from the membrane, it is possible to use optode at least 10 times. Membranes that were used and left to dry out typically for cellulose triacetate material undergo deformation, losing their mechanical properties (mainly flexibility). Thus between measurements optodes should be kept in solution, preferentially in regeneration solution. Just prepared optodes and not used for measurements can be stored safely for a period of at least 3 months in a dry and dark place (room conditions) without losing their properties. Fig. 22b shows the influence of addition of equimolar, 10-fold and 100-fold molar excess of interfering ions salt on the spectral response of optodes immersed in 10^{-5} M solution of copper(II) chloride. RR% value does not exceed 5% even in 100-fold molar excess of interfering ions and their mixture.
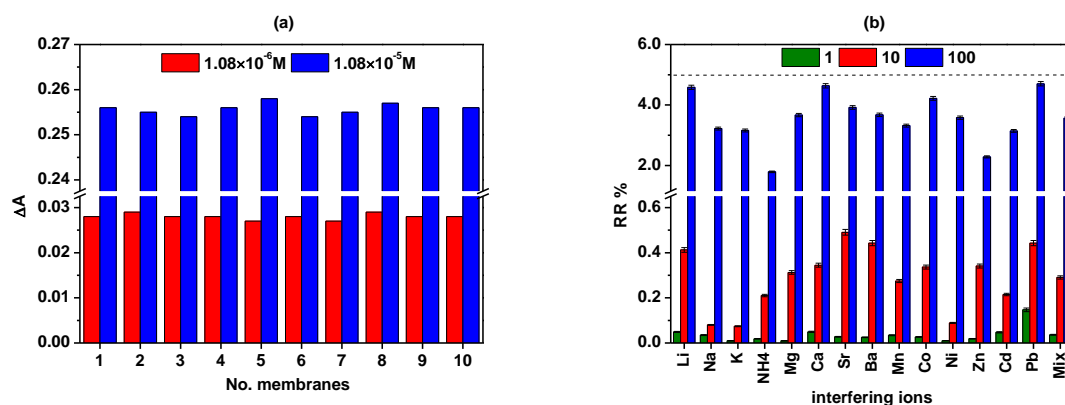
Fig. 22. (a) Reproducibility of optode after contact with copper(II) chloride solution (pH 5.0) and (b) interferences of several metal chlorides used at equimolar, 10-fold and 100-fold molar excess, expressed as RR%, to spectral response (ΔA) of optodes (at 540 nm) towards copper(II) chloride (pH 5.0).

Fig. 23 shows color changes of optodes with **L** after contact with increasing concentration of copper(II) chloride at pH 5.0. Naked-eye color changes were observed above 10^{-6} M of copper(II) chloride.

Fig. 23. Color changes of optode upon titration with copper(II) chloride (c_{Cu} = 0-3.36×10⁻⁴ M) at pH 5.0.

The colorimetric analysis of the digital images was carried out in parallel with the studies of the spectrophotometric response of the optodes. Fig. 24 shows these correlations in DMSO:SBF 1:9 (v/v) solution. The widest range of the linear response $2.16×10^{-7}$ –$1.72×10^{-4}$ M (R^2 = 0.9879) was obtained for R/G color ratio with detection limit $8.27×10^{-7}$ M, but the lowest LOD $4.06×10^{-7}$ M was obtained for color change ΔE_{RGB} with linear response $4.31×10^{-7}$ – $2.48×10^{-5}$ M (R^2 = 0.9993). All investigated color dependences for discussed optodes with concentration of copper(II) chloride are collected in Table S4.
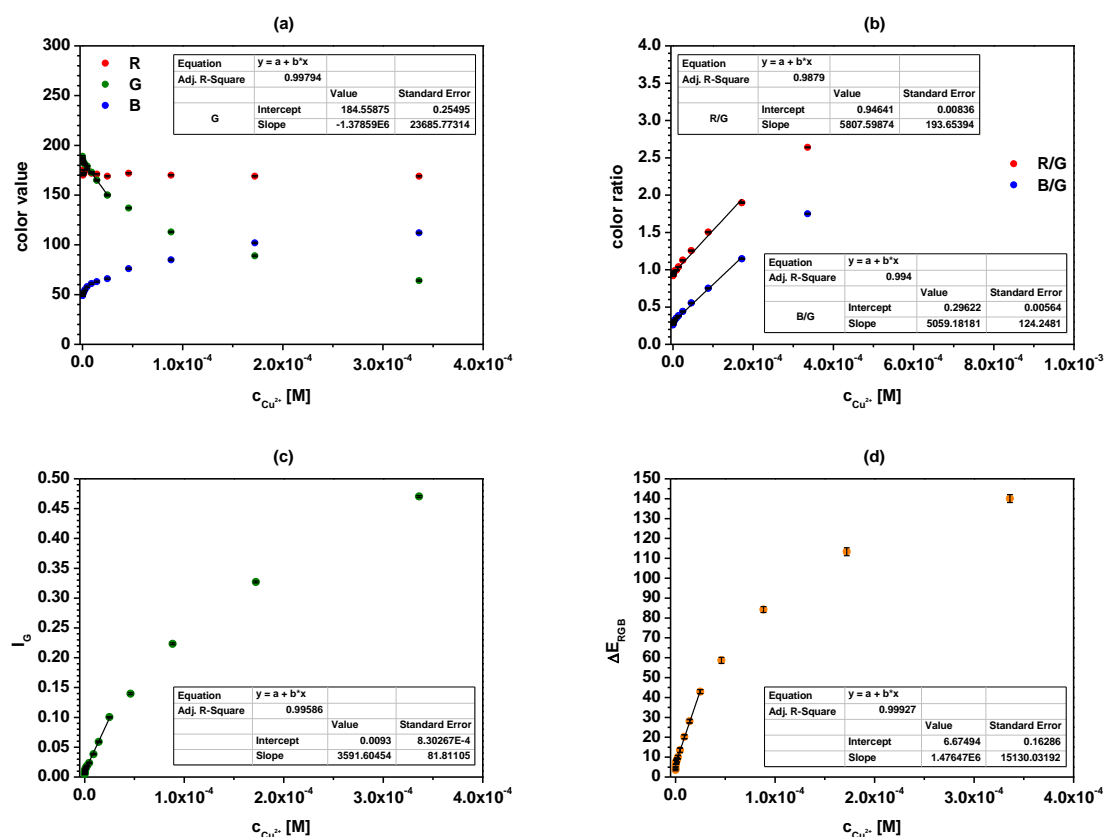
Fig. 24. Dependence of (a) color value; (b) color ratio (R/G, B/G); (c) color intensity (I_G) and (d) color change (ΔE_{RGB}) of optode with **L** upon titration with copper(II) chloride (c_{Cu} = 0-4.28×10⁻⁵ M) at pH 5.0.

In Table 4 the properties of copper(II) selective optodes obtained in recent years and described in literature [96-99] are listed for comparison with the characteristics of optode with **L**. From this comparison it is quite well seen that optode obtained by us is, in general, more or

less comparable with those proposed by other authors. The advantage is the use of a biodegradable polymer matrix that does not require additional support in the form of glass and the possibility of colorimetric determination of copper(II) ions using a Smartphone.

Table 4. Comparison of obtained optode with already existing ones

Sensing material	Support	pH	Response time	Linear response [M]	LOD [M]	Reference
EBSI [a]	PVC	4.0	3 min	$1.57 \times 10^{-7} – 5.04 \times 10^{-4}$	1.26×10^{-7}	[96]
HIBIN	Sol-gel	5.0	2 min	$9.10 \times 10^{-8} – 1.12 \times 10^{-5}$	1.80×10^{-8}	[97]
Schiff base	Sol-gel	5.5	2 min	$8.54 \times 10^{-8} – 1.00 \times 10^{-5}$	1.53×10^{-8}	[98]
Schiff base	PVA/TEOS	5.0	1.5 min	$9.34 \times 10^{-8} – 1.15 \times 10^{-5}$	1.27×10^{-8}	[99]
L	CTA	5.0	2-4 min	$5.41 \times 10^{-8} – 2.48 \times 10^{-5}$	7.22×10^{-8}	This work
				$4.31 \times 10^{-7} – 2.48 \times 10^{-5}$	$4.06 \times 10^{-7 \text{ b}}$	

[a] N,N'-(4,40-ethylene biphenyl)bis(3-methoxy salicylidineimine)
[b] Smartphone detection

3.14. Determination of copper(II) in model and real samples.

Possible application of proposed chemosensor **L** and optode were tested using different samples: of known copper(II) concentrations – commercial copper(II) standard solution, spiked tap water from different regions of northern Poland, commercial drinking water samples and Qnova calibration solution. In the last case results were compared with the values obtained by independent analysis using ICP-OES. All measurements were done at pH 5.0. Both attempts were tested: spectrophotometric and colorimetric detection of copper(II).

Comparison of recovery results obtained for chemosensor **L** in solution and optodes upon immersion of the sensor layer in a commercial standard reference solution of copper(II) for different concentrations in range from 4.46×10^{-7} to 1.32×10^{-5} M are collected in Table 5. The recoveries are at least about 98.96 - 99.96 % and 95.56 - 100.18 % for spectrophotometric detection (ΔA) for **L** and optode, respectively.

Table 5. Determination of copper(II) ions - recovery test for commercial standard solution.

Standard reference solution of copper(II) [M]	**L**		Optode	
	Found copper(II) [M]	Recovery [%]	Found copper(II) [M]	Recovery [%]
4.46×10^{-7}	$4.38 \times 10^{-7} \pm 3.11 \times 10^{-8}$	98.21 ± 6.97	$4.26 \times 10^{-7} \pm 3.68 \times 10^{-8}$	95.56 ± 8.25
8.92×10^{-7}	$8.92 \times 10^{-7} \pm 3.10 \times 10^{-8}$	99.96 ± 2.93	$8.85 \times 10^{-7} \pm 3.26 \times 10^{-8}$	99.19 ± 3.66
2.67×10^{-6}	$2.66 \times 10^{-6} \pm 3.08 \times 10^{-8}$	99.63 ± 1.15	$2.67 \times 10^{-6} \pm 3.19 \times 10^{-8}$	100.07 ± 1.20
4.45×10^{-6}	$4.42 \times 10^{-6} \pm 3.83 \times 10^{-8}$	99.37 ± 0.86	$4.44 \times 10^{-6} \pm 6.48 \times 10^{-8}$	99.82 ± 1.45
8.85×10^{-6}	$8.80 \times 10^{-6} \pm 7.66 \times 10^{-8}$	99.41 ± 0.87	$8.87 \times 10^{-6} \pm 8.08 \times 10^{-8}$	100.18 ± 0.91
1.32×10^{-5}	$1.31 \times 10^{-5} \pm 8.94 \times 10^{-8}$	99.55 ± 0.68	$1.32 \times 10^{-5} \pm 1.10 \times 10^{-7}$	99.85 ± 0.83

To evaluate the influence of the sample matrix three different samples of tap water and three samples of drinking water were spiked with known concentration of copper(II) - Table 6. In this case ΔA recoveries were within 98.58 – 101.92 % and 97.05 – 101.35 % for solution of

29

L and optode, respectively. Elemental composition of drinking water samples was included in the Table S5.

Table 6. Determination of copper(II) ions in a real sample - spiked tap water and drinking water.

Real sample	Added copper(II) [M]	L		Optode	
		Found copper(II) [M]	Recovery [%]	Found copper(II) [M]	Recovery [%]
Tap water 1	0	$4.12 \times 10^{-7} \pm 3.11 \times 10^{-8}$	-	$3.91 \times 10^{-7} \pm 7.07 \times 10^{-8}$	-
	4.46×10^{-7}	$8.21 \times 10^{-7} \pm 3.65 \times 10^{-8}$	99.32 ± 4.44	$8.12 \times 10^{-7} \pm 5.56 \times 10^{-8}$	97.05 ± 6.85
	4.45×10^{-6}	$4.85 \times 10^{-6} \pm 3.40 \times 10^{-8}$	100.59 ± 0.70	$4.80 \times 10^{-6} \pm 7.28 \times 10^{-8}$	99.24 ± 1.52
	1.10×10^{-5}	$1.15 \times 10^{-5} \pm 2.76 \times 10^{-8}$	100.31 ± 0.24	$1.14 \times 10^{-5} \pm 5.70 \times 10^{-8}$	100.14 ± 0.50
Tap water 2	0	$1.33 \times 10^{-6} \pm 3.32 \times 10^{-8}$	-	$1.29 \times 10^{-6} \pm 1.67 \times 10^{-7}$	-
	4.46×10^{-7}	$1.79 \times 10^{-6} \pm 7.09 \times 10^{-8}$	101.40 ± 3.96	$1.71 \times 10^{-6} \pm 6.75 \times 10^{-8}$	98.57 ± 3.95
	4.45×10^{-6}	$5.79 \times 10^{-6} \pm 3.42 \times 10^{-8}$	100.36 ± 0.59	$5.78 \times 10^{-6} \pm 7.29 \times 10^{-8}$	100.74 ± 1.26
	1.10×10^{-5}	$1.24 \times 10^{-5} \pm 3.60 \times 10^{-8}$	99.91 ± 0.29	$1.23 \times 10^{-5} \pm 7.19 \times 10^{-8}$	99.98 ± 0.58
Tap water 3	0	$1.01 \times 10^{-6} \pm 2.63 \times 10^{-8}$	-	$1.02 \times 10^{-6} \pm 1.34 \times 10^{-7}$	-
	4.46×10^{-7}	$1.45 \times 10^{-6} \pm 5.63 \times 10^{-8}$	100.05 ± 3.88	$1.45 \times 10^{-6} \pm 6.98 \times 10^{-8}$	98.92 ± 4.80
	4.45×10^{-6}	$5.45 \times 10^{-6} \pm 3.54 \times 10^{-8}$	100.00 ± 0.65	$5.42 \times 10^{-6} \pm 7.28 \times 10^{-8}$	99.17 ± 1.34
	1.10×10^{-5}	$1.21 \times 10^{-5} \pm 3.39 \times 10^{-8}$	100.09 ± 0.28	$1.22 \times 10^{-5} \pm 5.87 \times 10^{-8}$	100.93 ± 0.48
Drinking water 1	0	<LOD	-	<LOD	-
	4.46×10^{-7}	$4.47 \times 10^{-7} \pm 2.26 \times 10^{-8}$	100.25 ± 5.05	$4.52 \times 10^{-7} \pm 2.17 \times 10^{-8}$	101.35 ± 4.80
	4.45×10^{-6}	$4.43 \times 10^{-6} \pm 4.02 \times 10^{-8}$	99.64 ± 0.91	$4.47 \times 10^{-6} \pm 4.76 \times 10^{-8}$	100.46 ± 1.07
	1.10×10^{-5}	$1.11 \times 10^{-5} \pm 5.49 \times 10^{-8}$	100.69 ± 0.49	$1.11 \times 10^{-5} \pm 7.82 \times 10^{-8}$	100.90 ± 0.70
Drinking water 2	0	<LOD	-	<LOD	-
	4.46×10^{-7}	$4.40 \times 10^{-7} \pm 2.67 \times 10^{-8}$	98.58 ± 6.06	$4.35 \times 10^{-7} \pm 2.79 \times 10^{-8}$	97.41 ± 6.43
	4.45×10^{-6}	$4.43 \times 10^{-6} \pm 6.14 \times 10^{-8}$	99.30 ± 1.39	$4.46 \times 10^{-6} \pm 5.83 \times 10^{-8}$	100.26 ± 1.31
	1.10×10^{-5}	$1.11 \times 10^{-5} \pm 7.22 \times 10^{-8}$	100.42 ± 0.65	$1.11 \times 10^{-5} \pm 9.58 \times 10^{-8}$	100.82 ± 0.86
Drinking water 3	0	<LOD	-	<LOD	-
	4.46×10^{-7}	$4.55 \times 10^{-7} \pm 2.68 \times 10^{-8}$	101.92 ± 5.89	$4.44 \times 10^{-7} \pm 1.77 \times 10^{-8}$	99.38 ± 3.99
	4.45×10^{-6}	$4.45 \times 10^{-6} \pm 4.92 \times 10^{-8}$	100.14 ± 1.11	$4.48 \times 10^{-6} \pm 4.34 \times 10^{-8}$	100.66 ± 0.97
	1.10×10^{-5}	$1.11 \times 10^{-5} \pm 6.93 \times 10^{-8}$	100.96 ± 0.62	$1.11 \times 10^{-5} \pm 6.91 \times 10^{-8}$	100.58 ± 0.62

The last probe for testing practical application of the proposed chemosensor and sensor layer for spectrophotometric detection of copper(II) in a complex matrix was carried out using Qnova calibration solution. The elemental composition of the Qnova calibration solution is shown in Table S6. Trace elements were determined by the ICP-OES method. In Table 7 results of the recovery test are collected. The spectrophotometric (ΔA) recoveries were 97.63 - 99.50 % and 94.83 - 99.32 % for **L** in solution and optode, respectively

Table 7. Spectrophotometric determination of copper(II) ions in Qnova calibration solution

	ICP-OES	Added copper(II) [M]	L		Optode	
			Found copper(II) [M]	Recovery [%]	Found copper(II) [M]	Recovery [%]
Qnova calibration solution	$2.36\times10^{-7}\pm1.18\times10^{-8}$	0	$2.30\times10^{-7}\pm1.65\times10^{-8}$	97.63 ± 7.01	$2.24\times10^{-7}\pm1.97\times10^{-8}$	94.83 ± 8.34
		4.46×10^{-7}	$6.75\times10^{-7}\pm4.05\times10^{-8}$	99.03 ± 5.94	$6.63\times10^{-7}\pm3.68\times10^{-8}$	97.18 ± 5.40
		4.45×10^{-6}	$4.65\times10^{-6}\pm4.38\times10^{-8}$	99.19 ± 0.93	$4.64\times10^{-6}\pm9.78\times10^{-8}$	99.06 ± 2.09
		1.10×10^{-5}	$1.12\times10^{-5}\pm8.37\times10^{-8}$	99.50 ± 0.74	$1.12\times10^{-5}\pm1.14\times10^{-7}$	99.32 ± 1.01

4. Conclusion

New *o*-hydroxyazocompound **L** bearing pyrrole moiety was obtained in a facile procedure. It was found that this simple compound has interesting properties in solution and in a solid state. Detailed studies of metal cation complexation by **L** allow to conclude that this easily available compound can serve as an effective spectrophotometric reagent for detection and determination of copper(II) in samples of various compositions. On the other hand, simple sensing materials based on **L** selectively generate colorimetric signal in the presence of copper(II), which can be used for non-instrumental detection of this important metal cation. The second option is using a mobile device camera as a detector. The characteristics of the above systems such as linear response range, limit of detection, possibility of regeneration etc. make them useful for wireless routine analysis of environmental and biological samples in laboratories and field analysis.

Appendix A. Supplementary material

Supplementary data to this article can be found online at…

Crystallographic data for all structures reported in this paper have been deposited with the Cambridge Crystallographic Data Centre as supplementary publication No. CCDC 2190550. The data can be obtained free of charge from The Cambridge Crystallographic Data Centre via www.ccdc.cam.ac.uk/structures.

Declaration of Competing Interest

The authors declare that they have no known competing financial interests or personal relationships that could have appeared to influence the work reported in this paper.

CRediT author statement

Błażej Galiński: Conceptualization, Data curation, Formal analysis, Investigation, Methodology, Project administration, Validation, Visualization, Writing – original draft, Writing – review & editing; Jarosław Chojnacki: Data curation, Investigation, Methodology, Visualization, Writing – original draft; Ewa Wagner-Wysiecka: Conceptualization, Data

31

curation, Supervision, Validation, Visualization, Writing – original draft, Writing – review & editing. All the authors discuss the results and commented on the manuscript.

Acknowledgments

References

[1] H. Tapiero, D.M. Townsend, K.D. Tew, Trace elements in human physiology and pathology. Copper, Biomed. Pharmacother. 57 (2003) 386-398.

[2] B.-E. Kim, T. Nevitt, D.J. Thiele, Mechanisms for copper acquisition, distribution and regulation, Nat. Chem. Biol. 4 (2008) 176-185.

[3] R.A. Festa, D.J. Thiele, Copper: An essential metal in biology, Curr. Biol. 21 (2011) 877–883.

[4] T. Tsang, C.I. Davis, D.C. Brady, Copper biology, Curr. Biol. 31 (2021) 421-427.

[5] O. Bandmann; K.H. Weiss, S.G. Kaler, Wilson's disease and other neurological copper disorders, Lancet Neurol. 14 (2015) 103-113.

[6] A. Członkowska, T. Litwin, P. Dusek, P. Ferenci, S. Lutsenko, V. Medici, J.K. Rybakowski, K.H. Weiss, M.L. Schilsky, Wilson disease, Nat. Rev. Dis. Prim. 4 (2018) 21.

[7] T. Fukai, M. Ushio-Fukai, J.H. Kaplan, Copper transporters and copper chaperones: Roles in cardiovascular physiology and disease, Am. J. Physiol. Cell Physiol. 315 (2018) 186-201.

[8] M. Siotto, R. Squitti, Copper imbalance in Alzheimer's disease: Overview of the exchangeable copper component in plasma and the intriguing role albumin plays, Coord. Chem. Rev. 371 (2018) 86-95.

[9] T.J. Huat, J. Camats-Perna, E.A. Newcombe, N. Valmas, M. Kitazawa, R. Medeiros, Metal toxicity links to Alzheimer's disease and neuroinflammation, J. Mol. Biol. 431 (2019) 1843-1868.

[10] M. Altarelli, N. Ben-Hamouda, A. Schneider, M.M. Berger, Copper deficiency: Causes, manifestations, and treatment, Nutr. Clin. Pract. 34 (2019) 504-513.

[11] M. Rehman, L. Liu, Q. Wang, M.H. Saleem, S. Bashir, S. Ullah, D. Peng, Copper environmental toxicology, recent advances, and future outlook: A review, Environ. Sci. Pollut. Res. 26 (2019) 18003–18016.

[12] M.I. El Sabry, F.K.R. Stino, W.A.A. El-Ghany, Copper: benefits and risks for poultry, livestock, and fish production, Trop. Anim. Health Prod. 53 (2021) 487.

[13] V. Kumar, S. Pandita, G.P. Singh Sidhu, A. Sharma, K. Khanna, P. Kaur, A.S. Bali, R. Setia, Copper bioavailability, uptake, toxicity and tolerance in plants: A comprehensive review, Chemosphere 262 (2021) 127810.

[14] World Health Organization. Guidelines for drinking-water quality: fourth edition incorporating the first and second addenda. Geneva, 2022.

[15] S. Carter, A. Fisher, B. Gibson, J. Marshall, B. Russelle, I. Whitesidef, Atomic spectrometry update: Review of advances in the analysis of metals, chemicals and materials, J. Anal. At. Spectrom. 32 (2017) 2068-2117.

[16] Y. Lu, X. Liang, C. Niyungeko, J. Zhou, J. Xu, G. Tian, A review of the identification and detection of heavy metal ions in the environment by voltammetry, Talanta 178 (2018) 324-338.

[17] S.-H. Chen, Y.-X. Li, P.-H. Li, X.-Y. Xiao, M. Jiang, S.-S. Li, W.-Y. Zhou, M. Yang, X.-J. Huang, W.-Q. Liu, Electrochemical spectral methods for trace detection of heavy metals: a review, Trends Anal. Chem. 106 (2018) 139-150.

[18] J. Dalmieda, P. Kruse, Metal cation detection in drinking water, Sensors 19 (2019) 5134.

[19] Q. Ding, C. Li, H. Wang, C. Xu, H. Kuang, Electrochemical detection of heavy metal ions in water, Chem. Commun. 57 (2021) 7215-7231.

[20] S. Sharma, K.S. Ghosh, Recent advances (2017–20) in the detection of copper ion by using fluorescence sensors working through transfer of photo-induced electron (PET), excited-state intramolecular proton (ESIPT) and Forster resonance energy (FRET), Spectrochim. Acta A Mol. Biomol. Spectrosc. 254 (2021) 119610.

[21] T. Chopra, S. Sasan, L. Devi, R. Parkesh, K.K. Kapoor, A comprehensive review on recent advances in copper sensors, Coord. Chem. Rev. 140 (2022) 214704.

[22] M. Saleema, K.H. Lee, Optical sensor: a promising strategy for environmental and biomedical monitoring of ionic species, RSC Adv. 5 (2015) 72150-72287.

[23] L. You, D. Zha, E.V. Anslyn, Recent advances in supramolecular analytical chemistry using optical sensing, Chem. Rev. 115 (2015) 7840–7892.

[24] J. Wu, B. Kwon, W. Liu, E.V. Anslyn, P. Wang, J.S. Kim, Chromogenic/Fluorogenic ensemble chemosensing systems, Chem. Rev. 115 (2015) 7893–7943.

[25] H. Sharma, N. Kaur, A. Singh, A. Kuwar, N. Singh, Optical chemosensors for water sample analysis, J. Mater. Chem. C 4 (2016) 5154-5194.

[26] P.V.S. Ajay, J. Printo, D.S.C.G. Kiruba, L. Susithra, K. Takatoshi, M. Sivakumar Colorimetric sensors for rapid detection of various analytes, Mater. Sci. Eng. C 78 (2017) 1231-1245.

[27] I.V. Kolesnichenko, E.V. Anslyn, Practical applications of supramolecular chemistry, Chem. Soc. Rev. 46 (2017) 2385-2390.

[28] Y. Ma, Y. Li, K. Ma, Z. Wang, Optical colorimetric sensor arrays for chemical and biological analysis, Sci. China Chem. 61 (2018) 643–655.

[29] I.I. Ebralidze, N.O. Laschuk, J. Poisson, O.V. Zenkina, Colorimetric sensors and sensor arrays, in: Zenkina, O.V. (Eds.), Nanomaterials Design for Sensing Applications, Elsevier, 2019, pp. 1-39.

[30] G. Fukuhara, Analytical supramolecular chemistry: Colorimetric and fluorimetric chemosensors, J. Photochem. Photobiol. C: Photochem. Rev. 42 (2020) 100340.

[31] P.R. Dongare, A.H. Gore, Recent advances in colorimetric and fluorescent chemosensors for ionic species: design, principle and optical signalling mechanism, ChemistrySelect 6 (2021) 5657-5669.

[32] J. Kramer, R. Kang, L.M. Grimm, L. De Cola, P. Picchetti, F. Biedermann, Molecular probes, chemosensors, and nanosensors for optical detection of biorelevant molecules and ions in aqueous media and biofluids, Chem. Rev. 122 (2022) 3459–3636.

[33] H.N. Kim, W.X. Ren, J.S. Kim, J. Yoon, Fluorescent and colorimetric sensors for detection of lead, cadmium, and mercury ions, Chem. Soc. Rev. 41 (2012) 3210-3244.

[34] D. Udhayakumari, S. Nahaa, S. Velmathi, Colorimetric and fluorescent chemosensors for Cu2+. A comprehensive review from the years 2013–15, Anal. Methods 9 (2017) 552-578.

[35] B. Kaur, N. Kaur, S. Kumar, Colorimetric metal ion sensors – A comprehensive review of the years 2011–2016, Coord. Chem. Rev. 358 (2018) 13-69.

[36] A. Patil, S. Salunke-Gawali, Overview of the chemosensor ligands used for selective detection of anions and metal ions (Zn^{2+}, Cu^{2+}, Ni^{2+}, Co^{2+}, Fe^{2+}, Hg^{2+}), Inorg. Chim. Acta 482 (2018) 99-112.

[37] S. Upadhyay, A. Singh, R. Sinha, S. Omer, K. Negi, Colorimetric chemosensors for d-metal ions: A review in the past, present and future prospect, J. Mol. Struct. 1193 (2019) 89-102.

[38] S. Chakraborty, V. Ravindran, P.V. Nidheesh, S. Rayalu, Optical sensing of copper and its removal by different environmental technologies, ChemistrySelect 5 (2020) 10432-10474.

[39] A. Roy, M. Nandi, P. Roy, Dual chemosensors for metal ions: A comprehensive review, Trends Anal. Chem. 138 (2021) 116204.

[40] A. Lobnik, M. Turel, S.K. Urek, Optical chemical sensors: design and applications, in: Wang, W. (Eds.), Advances in Chemical Sensors, InTech, 2012, pp. 3-28.

[41] G. Mistlberger, G.A. Crespo, E. Bakker, Ionophore-based optical sensors, Annu. Rev. Anal. Chem. 7 (2014) 483-512.

[42] X. Xie, E. Bakker, Ion selective optodes: From the bulk to the nanoscale, Anal. Bioanal. Chem. 407 (2015) 3899-3910.

[43] K.N. Mikhelson, M.A. Peshkova, Advances and trends in ionophore-based chemical sensors, Russ. Chem. Rev. 84 (2015) 555-578.

[44] X. Du, X. Xie, Ion-Selective optodes: Alternative approaches for simplified fabrication and signaling, Sens. Actuators B Chem. 335 (2021) 129368.

[45] E, Wagner-Wysiecka, N. Łukasik, J.F. Biernat, E. Luboch, Azo group(s) in selected macrocyclic compounds, J. Incl. Phenom. Macrocycl. Chem. 90 (2018) 189-257.

[46] H. Chen, W. Chen, Y. Lin, Y. Xie, S.H. Liu, J. Yin, Visible and near-infrared light activated azo dyes, Chin. Chem. Lett. 32 (2021) 2359-2368.

[47] R.I. Alsantali, Q.A. Raja, A.Y.A. Alzahrani, A. Sadiq, N. Naeem, E.U. Mughal, M.M. Al-Rooqi, N. El Guesmi, Z. Moussa, S.A. Ahmed, Miscellaneous azo dyes: A comprehensive review on recent advancements in biological and industrial applications. Dyes Pigm. 199 (2022) 110050.

[48] R. Nagarajan, C. Varadaraju, K.H. Lee, Recent advancements in the role of N-Heterocyclic receptors on heavy metal ion sensing, Dyes Pigm. 91 (2021) 109331.

[49] F. Ahmed, H. Xiong, Recent developments in 1,2,3-triazole-based chemosensors, Dyes Pigm. 185 (2021) 108905.

[50] X. Wang, C. Shen, C. Zhou, Y. Bu, X. Yan, Methods, principles and applications of optical detection of metal Ios, Chem. Eng. J., 417 (2021) 129125.

[51] K.E. McCrackena, J.-Y. Yoon, Recent approaches for optical smartphone sensing in resource-limited settings: a brief review, Anal. Methods 8 (2016) 6591-6601.

[52] M. Rezazadeh, S. Seidi, M. Lid, S. Pedersen-Bjergaard, Y. Yamini, The modern role of smartphones in analytical chemistry, Trends Anal. Chem. 118 (2019) 548-555.

[53] S. Di Nonno, R. Ulber, Smartphone-based optical analysis systems, Analyst 146 (2021) 2749-2768.

[54] R. Sivakumar, N.Y. Lee, Recent progress in smartphone-based techniques for food safety and the detection of heavy metal ions in environmental water, Chemosphere 275 (2021) 130096.

[55] L.F. Capitán-Vallvey, N. López-Ruiz, A. Martínez-Olmos, M.M. Erenas, A.J. Palma, Recent developments in computer vision-based analytical chemistry: A tutorial review, Anal. Chim. Acta 899 (2015) 23-56.

[56] D. Yusufu, A. Mills, Spectrophotometric and digital colour colourimetric (DCC) analysis of colour-based indicators, Sensor. Actuators B Chem. 273 (2018) 1187-1194.

[57] A.V. Kalinichev, N.V. Pokhvishcheva, M.A. Peshkova, Novel color standards for digital color analysis of optochemical sensor arrays, Talanta 197 (2019) 638-644.

[58] G.M. Fernandes, W.R. Silva, D.N. Barreto, R.S. Lamarca, P.C.F. Lima Gomes, J.F.D.S. Petruci, A.D. Batista, Novel approaches for colorimetric measurements in analytical chemistry – A review, Anal. Chim. Acta 1135 (2020) 187-203.

[59] R. Jain, A. Thakur, P. Kaur, K.-H. Kim, P. Devi, Advances in imaging-assisted sensing techniques for heavy metals in water: Trends, challenges, and opportunities, Trends Anal. Chem. 123 (2020) 115758.

[60] N.Y. Tiuftiakov, A.V. Kalinichev, N.V. Pokhvishcheva, M.A. Peshkova, Digital color analysis for colorimetric signal processing: Towards an analytically justified choice of acquisition technique and color space, Sens. Actuators B Chem. 344 (2021) 130274.

[61] K. Koren, S.E. Zieger, Optode based chemical imaging—Possibilities, challenges, and new avenues in multidimensional optical sensing, ACS Sens. 6 (2021) 1671-1680.

[62] Y. Fan, J. Li, Y. Guo, L.;Xie, G. Zhang, Digital image colorimetry on smartphone for chemical analysis: A review, Measurement 171 (2021) 108829.

[63] O. Dinten, U.E. Spichiger, N. Chaniotakis, P. Gehrig, B. Rusterholz, W.E. Morf, W. Simon, Lifetime of neutral-carrier-based liquid membranes in aqueous samples and blood and the lipophilicity of membrane components, Anal. Chem. 63 (1991) 596–603.

[64] E. Luboch, M. Jeszke, M. Szarmach, N. Łukasik, New bis(azobenzocrown)s with dodecylmethylmalonyl linkers as ionophores for sodium selective potentiometric sensors, J. Incl. Phenom. Macrocycl. Chem. 86 (2016) 323–335.

[65] B. Galiński, E. Luboch, J. Chojnacki, E. Wagner-Wysiecka, Novel diazocrowns with pyrrole residue as lead(II) colorimetric probes, Materials 14 (2021) 7239.

[66] O.V. Dolomanov, L. J. Bourhis, R. J. Gildea, J.A.K. Howard, H.J. Puschmann, OLEX2: a complete structure solution, refinement and analysis program, Appl. Crystallogr. 42 (2009) 339–341.

[67] G. M. Sheldrick, Crystal structure refinement with SHELXL, Acta Cryst. A 71 (2015) 3–8.

[68] T. Kokubo, H. Kushitani, S. Sakka, T. Kitsugi, T. Yamamuro, Solutions able to reproduce in vivo surface-structure changes in bioactive glass-ceramic A-W, J. Biomed. Mater. Res. 24 (1990) 721-734.

[69] Cold Spring Harbor Laboratory Press. Phosphate-buffered saline (PBS). Available online: http://cshprotocols.cshlp.org/content/2006/1/pdb.rec8247 (accessed on 16 August 2022).

[70] N. Sarigul, F. Korkmaz, I. Kurultak, A new artificial urine protocol to better imitate human urine, Sci. Rep. 9 (2019) 20159.

[71] M. Kyvala, I. Lukes, Program Package "OPIUM". Available online: https://web.natur.cuni.cz/~{}kyvala/opium.html (accessed on 16 August 2022)

[72] B. Galiński, E. Wagner-Wysiecka, Pyrrole bearing diazocrowns: Selective chromoionophores for lead(II) optical sensing, Sens. Actuators B Chem. 361 (2022) 131678.

[73] M.D. Abramoff, P.J. Magalhaes, S.J. Ram, Image processing with ImageJ, Biophotonics Int. 11 (2004) 36-42

[74] C.A. Schneider, W.S. Rasband, K.W. Eliceiri, NIH Image to ImageJ: 25 years of image analysis, Nat. Methods 9 (2012) 671-675.

[75] N.A. Gavrilenko, S.V. Muravyov, S.V. Silushkin, A.S. Spiridonovab, Polymethacrylate optodes: A potential for chemical digital color analysis, Measurement 51 (2014) 464-469.

[76] S. Erdemir, O. Kocyigit, S. Malkondu, Optical and quantitative detection of Ca^{2+} ion by an calix[4] arene-isophorone incorporated fluorometric and colorimetric probe, J. Photochem. Photobiol. A Chem. 425 (2022) 113713.

[77] S. Millefori, F. Zuccarello, A. Millefori, F. Guerrera, Tautomerism in arylazonaphthols by dipole moment analysis, Tetrahedron 30 (1974) 735-738.

[78] P. Ball, C.H. Nicholls, Azo-hydrazone tautomerism of hydroxyazo compounds—A review, Dyes Pigm. 3 (1982) 5-26.

[79] M.A. Rauf, S. Hisaindee, N. Saleh, Spectroscopic studies of keto–enol tautomeric equilibrium of azo dye, RSC Adv. 5 (2015) 18097-18110.

[80] R. L. Reeves, R. S. Kaiser, Selective solvation of hydrophobic ions in structured solvents. Azo-hydrazone tautomerism of azo dyes in aqueous organic solvents, J. Org. Chem. 35 (1970) 3670-3675.

[81] X.-C. Chen, T. Tao, Y.-G. Wang, Y.-X. Peng, W. Huang, H.-F. Qian, Azo-hydrazone tautomerism observed from UV-vis spectra by pH control and metal-ion complexation for two heterocyclic disperse yellow dyes, Dalton Trans. 41 (2012) 11107-11115.

[82] L. Antonov, Tautomerism: methods and theories, Wiley-VCH, Weinheim, 2014.

[83] L. Antonov, Tautomerism: Concepts and Applications in Science and Technology, Wiley-VCH, Weinheim, 2016.

[84] Y. Li, B.O. Patrick, D. Dolphin, Near-Infrared absorbing azo dyes: Synthesis and X-ray crystallographic and spectral characterization of monoazopyrroles, bisazopyrroles, and a boron−azopyrrole complex, J. Org. Chem. 74 (2009) 5237.

[85] A. Ghanadzadeh Gilani, V. Taghvaei, E. Moradi Rufchahi, M. Mirzaei, Tautomerism, solvatochromism, preferential solvation, and density functional study of some heteroarylazo dyes, J. Mol. Liq. 273 (2019) 392 -407.

[86] D. Bialas, E. Kirchner, M.I.S. Röhr, F. Würthner, Perspectives in dye chemistry: A rational approach toward functional materials by understanding the aggregate state, J. Am. Chem. Soc. 143 (2021) 4500–4518.

[87] S. G. Muntean, G.M. Simu, L. Kurunczi, Z. Szabadai, investigation of the aggregation of three disazo direct dyes by Uv-Vis spectroscopy and mathematical analysis, Rev. Chim. (Bucureşti) 60 (2009) 152–155.

[88] J.A. Balam-Villarreal, B.J. López-Mayorga, D. Gallardo-Rosas, R.A. Toscano, M.P. Carreón-Castro, V.A. Basiuk, F. Cortés-Guzmán, J.G. López-Cortés, M.C. Ortega-Alfaro, π-Extended push-pull azo-pyrrole photoswitches: synthesis, solvatochromism and optical band gap, Org. Biomol. Chem. 18 (2020) 1657–1670.

[89] E. Haselbach, Electronenstruktur und physikalisch-chemische Eigenschaften von Azo-Verbindungen, Teil XV. Über die Struktur der protonierten Azobrücke in Azobenzolderivaten, Helv. Chim. Acta 53 (1970) 1526-1543.

[90] B. Bernet, A. Vasella ^{1}H-NMR analysis of intra- and intermolecular H-bonds of alcohols in DMSO: chemical shift of hydroxy groups and aspects of conformational analysis of selected monosaccharides, inositols, and ginkgolides, Helv. Chim. Acta 83 (2000) 995-1021.

[91] M. Verheijen, M. Lienhard, Y. Schrooders, O. Clayton, R. Nudischer, S. Boerno, B. Timmermann, N. Selevsek, R. Schlapbach, H. Gmuender, S. Gotta, J. Geraedts, R. Herwig, J. Kleinjans, F. Caiment, DMSO induces drastic changes in human cellular processes and epigenetic landscape in vitro, Sci. Rep. 9 (2019) 4641.

[92] I.J. Chang, M.G. Choi, Y.A. Jeong, S.H. Lee, S.-H. Chang, Colorimetric determination of Cu^{2+} in simulated wastewater using naphthalimide-based Schiff base, Tetrahedron Lett. 58 (2017) 474-477.

[93] T. Anand, S.K. Sahoo, Cost-effective approach to detect Cu(II) and Hg(II) by integrating a smartphone with the colorimetric response from a NBD-benzimidazole based dyad, Phys. Chem. Chem. Phys. 21 (2019) 11839.

[94] Y. Cao, Y. Liu, F. Li, S. Guo, Y. Shui, H. Xue, L. Wang, Portable colorimetric detection of copper ion in drinking water via red beet pigment and smartphone, Microchem. J. 15 (2019) 104176.

[95] Z.-H. Zhao, Z.-L. Hu, X.-T. Zhang, Q.-X. Liu, A new tridentate fluorescent-colorimetric chemosensor for copper(II) ion, Tetrahedron 75 (2019) 130675.

[96] Z. Lashkari, M. Arvand, Sensitive and selective detection of trace copper in standard alloys, food and biological samples using a bulk optode based on N,N0-(4,40-ethylene biphenyl) bis(3-methoxy salicylidine imine) as neutral carrier, Spectrochim. Acta A Mol. Biomol. Spectrosc. 107 (2013) 280-288.

[97] S.A. Shahamirifard, M. Ghaedi, M. Montazerozohori, Design a sensitive optical thin film sensor based on incorporation of isonicotinohydrazide derivative in sol–gel matrix for determination of trace amounts of copper (II) in fruit juice: Effect of sonication time on immobilization approach, Ultrason. Sonochem. 42 (2018) 723-730.

[98] Z. Parsaeea, N. Karachi, R. Razavi, Ultrasound assisted fabrication of a novel optode base on a triazine based Schiff base immobilized on TEOS for copper detection, Ultrason. Sonochem. 47 (2018) 36-46.

[99] W. Gao, P. Haratipour, M.R.R. Kahkha, A. Tahvili, Ultrasound-electrospinning-assisted fabrication and sensing evaluation of a novel membrane as ultrasensitive sensor for copper (II) ions detection in aqueous environment, Ultrason. Sonochem. 44 (2018) 152-161.